Universita` degli Studi di Genova

Scuola di Dottorato in Neuroscienze

Curriculum di Scienze delle Attività Motorie e Sportive

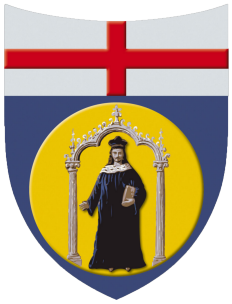

Shear wave elastography to assess the effect of botulinum toxin in muscle hypertonia following stroke

Candidate

Angelo Corazza

Tutor

Lucio Marinelli

Abstract

Introduction

Sonoelastography is a method capable of evaluating the mechanical properties of soft tissues by ultrasound (US). A further development of this technique is shear wave elastography (SWE), which provides a quantitative evaluation of the elastic properties - in terms of tissutal stiffness - by measuring the propagation velocities of the directional shear waves, produced by an ultrasound pulse.
Spasticity often appears in stroke patients in the affected limbs. It corresponds to velocity-dependent muscle hypertonia in relation to the hyperexcitability of the stretch reflex. Over time, the paretic muscles develop intrinsic alterations with consequent muscle shortening and increased fibrosis related to reduced use and immobilization.
Intramuscular injections of botulinum toxin A (BoNT-A) is an effective treatment which reduces muscle activity by inhibiting the release of acetylcholine at the neuromuscular junction level and is therefore able to reduce neuromediated muscle hypertonicity.
The study aims to evaluate the effectiveness of SWE to appreciate changes in stiffness in spastic muscles after treatment with BoNT-A and possibly detect differences between affected muscles and unaffected contralateral ones related to fibrous-fatty remodeling.

Materials & Methods

14 adult patients (5F; age: 58,4±14,1 years, m±SD; range:46-78) affected by spasticity were recruited after ischemic or hemorrhagic stroke diagnosed for at least 3 months and with a time interval from the last injection of at least 4 months, if already treated with BoNT-A. They patients underwent a physical examination in which muscle hypertonia was assessed using the modified Ashworth scale (MAS). The assessments were carried out on a sample muscle among the spastic ones favoring the greater volume and better accessibility to the ultrasound probe. SWE was also performed on the homologue non-paretic contralateral muscle. Spasticity was measured as the average electromyographic activity recorded during stretching (reflex by stretching) of the selected muscle at a reproducible speed, according to a previously validated methodology. The SWE evaluation was carried out with US scans across and along the direction of muscular fibers - as assessed by conventional US - covering the entire belly of the selected muscle to obtain a comprehensive estimate of the muscle stiffness both with the maximum shortened and elongated muscle position. Muscle fibrosis was also estimated on conventional B-mode US using the modified Heckmatt scale. All evaluations were performed shortly before botulinum toxin infiltration (T0) and one month later (T1). Clinical, electromyographic and ultrasound evaluation were performed by three different blinded examiners. Depending on data distribution, non-parametric statistical tests for paired data were performed for comparison; Spearman's r was calculated to assess data correlations.

Results

A total of 224 SWE values resulted considering both time points. Overall, SWE measurements on paretic muscles assessed with a longitudinal positioning of the probe showed statistically significant reduction at T1 versus T0 both in non stretched conditions ($p=0.001$) and in stretched conditions ($p=0.0029$).
After BoNT-A injection, a significant reduction in MAS ($p=0.009$), spastic dystonia ($p=0.0043$), spasticity ($p=0.0019$) and longitudinal SWE measurements, both in non stretched conditions ($p=0.001$) and in stretched conditions ($p=0.0029$), was observed. No significant changes in SWE parameters were observed on non-paretic versus contralateral muscle . All SWE measurements were higher in the paretic limb than in the contralateral one ($p<0.01$); higher SWE measurements resulted along the direction of muscular fibers versus across them ($p<0.01$). Cohen's *d* estimate a larger effect on EMG values than longitudinal SWE ones (either in non stretched and in stretched condition), with narrower 95%CI for SWE measurements. No changes resulted by the modified Heckmatt scale US assessments; there was a positive correlation (r: 0.46-0.84) between MHS scores and SWE values.

Conclusion

This is the first study evaluating the effect of BoNT-A on muscle hypertonia following stroke, assessed by mean of SWE and compared with the stretch reflex. The treatment resulted in a reduction of MAS, stretch reflex and muscular stiffness, in relation to the reduction of the neuro-mediated hypertonia. We have therefore shown that SWE is able to appreciate a reduction in neuro-mediated stiffness. Abolishing the neuro-mediated contribution by keeping the limb in a shortened position and moreover after BoNT-A injection, the SWE values resulted higher in the paretic muscle than in the healthy muscle in the same position. Hence, SWE-driven comparison between the spastic muscle and the contralateral unaffected homologous one is able to disclose the amount of stiffness due only to intrinsic muscular involutive remodeling. Alongside sEMG, SWE could therefore constitute an added-value to clinicians who manage spasticity for the assessment of responses to treatments and monitoring therapeutic interventions.

List of Abbreviations

ARF - Acoustic Radiation Force

ARFI - Acoustic Radiation Force Imaging

ARV - Average Rectified Value

BoNT-A - Botulinum NeuroToxin-A

FOV - Field Of View

KHz - KiloHertz

Kpa - Kilopascal

MAS - Modified Ashworth Scale

MHS - Modified Heckmatt scale

MHz - MegaHertz

mm - Millimeters

MRE - Magnetic Resonance Elastography

m/s - Meters per second

ROI - Region Of Interest

RF - Radiofrequency

SD - Standard Deviation

sEMG - Surface Electromyography

SEL - Sonoelastography

SWE - Shear Wave Elastography

THI - Tissue Harmonic Imaging

UMNS - Upper Motor Neuron Syndrome

US - Ultrasound

Contents

1. Ultrasound basic principles

Ultrasonography (US) is a well-established tomographic technique capable of providing a real-time representation of each human body structure, including moving structures. US clinical applications are continuously increasing thanks to its high sensitivity and image resolution, quickness, safety, portability and cost-effectiveness (Silvestri 2015).

In the past decade US become the referential imaging modality in the first level study of the soft-tissue components of the musculoskeletal system. Recent technological innovations improved image quality, reducing artefacts, and made possible the precise and accurate evaluation of almost all soft-tissue structures. Rapid advances in transducer technology (broadband and high definition probes), development of Tissue Harmonic Imaging (THI) systems, new dedicated software's and reconstruction algorithms (Compound imaging, Steering-Based imaging, Extended-Field-Of-View imaging, Three-Dimensional imaging, Sonoelastography), together with the possibility of a dynamic analysis of tendinous and muscular structures, resulted in increased diagnostic performances and opened new field of applications in the musculoskeletal area of interest.

In addition, it is important to highlight that US imaging has acquired a central role, not only in diagnostic phase, but also as an important guide for therapeutic manoeuvres such as biopsies of soft tissues, articular and periarticular infiltrative procedures, drainage of fluid collections and muscular haematomas.

As US examination is relatively operator-dependent, it presumes a good knowledge of the physical principles on which it bases on and the technical properties of the available equipment.

1.1 Ultrasound wave properties

Ultrasonography is based on the use of acoustic waves belong to the ultrasounds band. Ultrasounds are sounds possessing high frequencies, considerably higher than the human hearing range (> 20 kHz). Ultrasound waves propagate in the human body thanks to the elastic forces existing between the adjacent molecules of the encountered structures, as compression and rarefaction bands. (Fig.1).

Sound waves are mechanical pressure waves, produced by a disturbance source, that induce vibration of the particles of the material. Each particle swing, moving small distances from its rest position, so the vibrational energy is propagated from particle to particle as a wave travelling through the medium. On the basis of their relationship to the propagation direction of energy, sound waves are classified as being longitudinal or transverse waves, if the particles vibrate in the same direction or perpendicular to the propagation respectively. Longitudinal waves are tipically observed in soft tissues and liquids; the compact bone is the only tissue capable of supporting transverse sound waves (Silvestri 2015).

It is important to know the parameters characterizing an ultrasound wave: amplitude, frequency, wavelength, period, velocity, power and intensity (Tab. I).

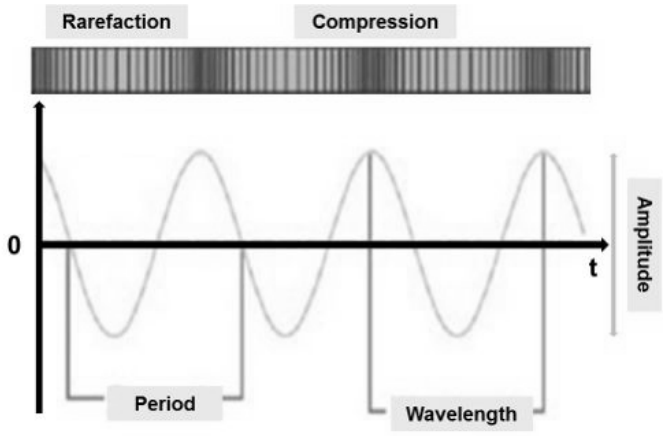

Fig. 1 The graphic demonstrates the oscillatory behaviour of the ultrasound waves propagating in tissues.

amplitude (A)	the maximum pressure value reached during the compression phase.
frequency (Y)	the number of cycles per unit of time (complete oscillations that each particle undergoes each second). Frequencies employed in diagnostic ultrasonography range from 1,5 to 20 MHz and sometimes higher. The high frequency of ultrasound waves is correlated to a very low wavelength; this properties guarantee the production of thin beam, well collimated, with a small divergence.
wavelength (λ)	the spatial interval in which each oscillatory phenomenon is reproduced. It is inversely proportional to frequency and influences the spatial resolution of the US image: the smaller the wavelength (corresponding to high frequency) the higher the spatial resolution; the greater the wavelength (corresponding to low frequency) the lower the spatial resolution.
period (ŧ)	the time interval in which each oscillatory phenomenon is reproduced.
velocity (v)	depends on the physical properties of the propagation medium. It varies in relation with tissue elasticity and density. Acoustic velocity is greater in rigid or less compressible materials, such as bone and metals, lower in air, water and soft tissues. The mean velocity in soft tissue (excluding bone and air) is 1540 m/s, the reference value used by manufacturers in the calibration of internal distance measurements.
power (P)	the total amount of energy passing through a surface per unit time (Watts).
intensity (I)	the strength of an ultrasound wave; it is the energy per unit area per unit time (Watts per square centimetre). Intensity changes depending on the width of the ultrasound beam; in focused beams it is greatest at the focus where the beam width is the narrowest.

Tab. I Main parameters that characterize an ultrasound wave.

1.2 Interactions between US and anatomical structures

In ultrasonography, high-frequency sound waves are generated and transmitted through the body by a transducer. When the US beam runs into a tissue target some of its energy is reflected back to the transducer, as a returning echo, some is deflected and continues its propagation into tissues. The transducer is responsible for both the production of the US beam and the detection of the returning echoes; it behave as an antenna that converts electrical pulses into the transmitted sound waves and receives the reflected and scattered ultrasound waves, converting them back into electrical signals, then encoded into images.

In travelling through the body, a sound wave is subjected to varying phenomena that contribute to US image formation: attenuation, absorption, reflection, diffusion, refraction and divergence.

Attenuation: is the continuous loss of acoustic energy (intensity) that the US beam undergoes running into tissues. It is usually expressed in units of decibels per centimetre and correlated to the US frequency (MHz) and the distance travelled (cm): the higher the frequency and the distance, the greater the attenuation. For this reason, although high frequency US allow a better image resolution, the US beam is more attenuated. This fact has an important practical implication: high- frequency linear-array probes (7-13 MHz) are used for the study of superficial structures (tendons, muscles, ligaments); low-frequency curved-array probes (2,5-5 MHz) are utilized for deep organs evaluation. The main causes of attenuation are absorption, reflection, refraction, diffusion and divergence.

Absorption: is the greatest cause of attenuation. The acoustic energy is transferred from the US beam to tissues and transformed into heat. The amount of absorption depends on US beam frequency and intrinsic characteristics of the medium (low in liquids, intermediate in soft tissues, high in bones and air).

Reflection: whenever the US beam encounters an interface between two materials

with different acoustic impedance, some of the energy is reflected (reflection) and the remainder is transmitted deviated through the interface (refraction), (Fig.1.2). The direction of the reflected wave (returning echo) depends on the orientation of sound wave relative to the surface: the angle of reflection equals the angle of incidence. The amplitude of the echo is directly correlated to: (a) the orientation of the US beam to the reflecting surface: reflection is greatest when the US beam is perpendicular to the surface (angle of incidence = zero), so produce the strongest detected echoes in clinical sonograms (*specular reflection*); (b) the relative difference in acoustic impedance between the tissues on either side of the interface: acoustic impedance is an intrinsic property of tissues which expresses their resistance to the passage of the US beam (expressed in units of Rayls = kilograms per square meter per second). The greater the difference in acoustic impedance between two materials, the stronger will be the intensity of the returning echo. Reflection can be either *specular* or *diffuse*, depending on the interface characteristics. When the interface is represented by a wide, smooth and homogeneous surface (diaphragm, vessel wall) the reflection is specular or mirror-like; when the interface shows a small, irregular and rough surface (parenchymal organs) the reflected wave will be diffuse.

Diffusion: is the scattering of the reflected US beam in all directions. It is typical of the parenchymal tissues, in which sound is scattered by the many cell and tissue elements that function as multiple interfaces.

Refraction: is the deviation of the transmitted beam from the incident beam direction. It increases as the angle of incidence is not perpendicular to the surface.

Divergence: if the US beam is not focused, tends to diverge distally with consequent reduction of the depth resolution.

1.3 Image formation

Ultrasonographic images are obtained with a pulse-echo type of measurement.

The transducer is an essential element of US equipment's. It is composed by a number of assembled crystals that are excited by electrical pulses (*piezoelectric effect* - applying an electric field to crystals causes their mechanical oscillations). Based on the pulse-echo principle occurring with piezoelectric crystals, US transducers convert electricity (electrical energy) into sound (mechanical energy).

The US waves, sent from the transducer, propagate through tissues and then return reflected as echoes to the transducer. Those returning echoes are then converted back into electrical pulses by the transducer crystals (*reverse piezoelectric effect* - converts mechanical energy, due to crystal deformation, into electrical energy) and are further processed in order to form the ultrasound image presented on the screen.

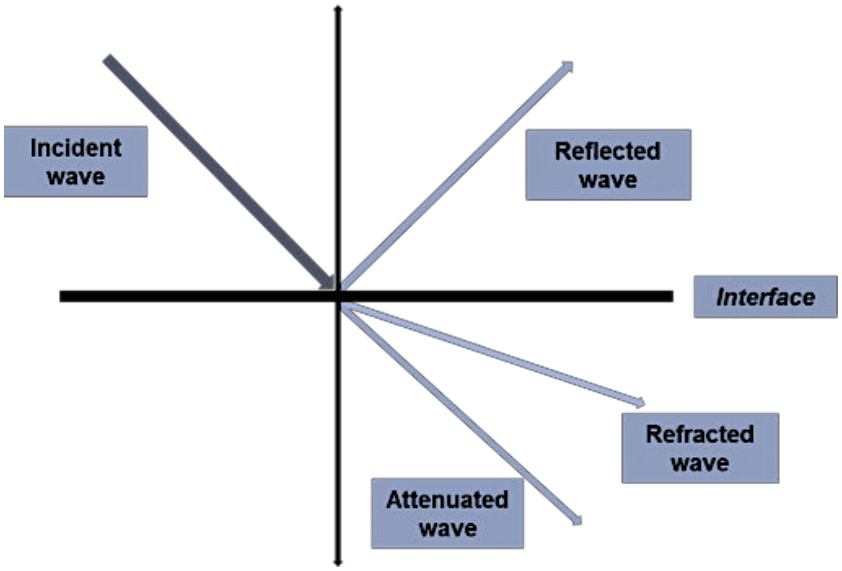

Fig. 2 Scheme of the physical phenomena contributing to US image formation.

The US beam is considered a combination of multiple thin beams produced by each crystal assembled in the transducer, with a linear or curved disposition. Currently, transducers contain a range of ultrasound frequencies (bandwidth) instead of a single fundamental frequency.

The generation of US images requires a complicated acquisition and display of ultrasound pulse-echo data. The broadband transducer generates a sequential series of focused beams all in the same plane (scan plane). Each set of target data from a single pulse transmission is placed in the image, as acquired along a line. All tissues in the scan plane are interrogated by these beams and each real-time image frame is composed of a set of parallel or sector lines representing the positions of the interrogating beams in the patient. Computer algorithms are used to fill in between the image lines so that the image appears continuous.

When the transmitted US pulse encounters internal tissue targets, part of its energy is deflected (reflected or scattered) back to the transducer (the echo). Because pulse-echo imaging techniques employ the same transducer for both sending and receiving US pulses, only echoes traveling in the direction of the transducer have any chance of being detected (Silvestri 2015).

The main pulse-echo parameters used in the formation of images include echo amplitude and target spatial position. Echo amplitude is encoded into shades of grey (grey-scale imaging), with the lighter shades representing higher amplitude echoes.

The depth of the target along the direction of the beam is accurately calculated from a pulse time-of-flight measurement. Assuming US propagation velocity is fairly constant from tissue to tissue (1540 m/s), the time between beam transmission and echo reception is used to determine the exact internal spatial location of all tissue targets.

Two important parameters representing image quality are:

Spatial resolution refers to the capability to distinguish two adjacent points, along the axis of the beam (axial resolution) or in a plane perpendicular to the axis of beam (lateral resolution).

Temporal resolution represents the capability of the US equipment to show anatomical structures in real time. It is related with the pulse repetition frequency (PRF) and with the frame (number of encoded images per unit time).

Visualization systems:

1. Amplitude mode (*A-mode*): the simplest form of display. It is a diagram in which echo amplitude is shown according to tissue depth (echo time of flight).

2. Time-motion mode (*TM-mode*): echoes returning from moving structures are displayed depending on the time. It is used in cardiac US evaluation.

3. Brightness mode (*B-mode*): grey-scale tomographic imaging commonly used in clinical practice.

1.4 US equipment

Good technical skills are essential in order to extract the maximum amount of information that can be obtained with the equipment, while avoiding the numerous pitfalls and artefacts of US imaging modality. Some important parameters can be adjusted before and during US examination in order to improve image quality and diagnostic performances.

Probe selection: high-frequency linear-array probes, operating with frequencies of 10 MHz or more, are mandatory for a precise evaluation of the soft-tissues of the musculoskeletal system (Fig. 3).

Fig. 3. Linear array probe with frequency range 5-12 MHz (left). Convex array probe with lower frequency range 2-5 MHz (right).

Beam focusing: determine the number and pattern of focal zones (zone in which the width and thickness of the US beam is reduced in order to increase contrast and spatial resolution). The focal depth can be changed dynamically during the examination.

Gain adjustment: optimize echoes intensity at different levels of depth.

Zoom: better visualize small and thin structures.

D*ynamic range adjustment*: set the contrast resolution. High values of the dynamic range allows for the visualization of very low-intensity echoes, reducing the contrast resolution; so the dynamic range must be reduced in order to enhance the contrast resolution.

1.5 Artifacts

Image artifacts (errors in image display) are common in clinical ultrasonography and can cause confusion for the interpreting physician. Some artefacts occur secondary to improper scanning technique; others are unavoidable because correlated to the physical characteristic of the US beam.

A detailed description of US artifacts lies outside the aim of this work. However, the knowledge of artifacts often encountered in US soft-tissue evaluation is essential to improve diagnostic performance.

Anisotropy is the intrinsic property of some anatomical structures to modify their reflecting capability in respect to the US beam angle of incidence. If the US beam not perpendicularly encounters linear structures, such as muscles, tendons and ligaments, the reflection isn't specular so the returning echoes have low intensity: the structure wrongly appears more hypoechoic (the artifact results with a loss of echogenicity in structure). (Fig. 8) The ability to recognize and correct anisotropy artifacts is important for image quality improvement and optimal patient care.

1.6 US of muscles

Selection of the proper transducer and US parameters are important aspects of muscle ultrasonography and depends on the depth and size of the muscle in exam.

For superficial muscles high-frequency (*7–15 MHz*) linear transducers are most useful and provides a good balance between tissues penetration and resolution; however, a correct examination of deeper structures sometimes requires a lower-frequency convex transducers (*3-10 MHz*). (Fig. 3)

US muscles appearance is predominately hypoechoic with hyperechoic septations: muscle bundles are hypoechoic in comparison to subcutaneous fat and are separated by the hyperechogenic fibroadipose perimysium septa (Pillen 2010) (Fig. 4).

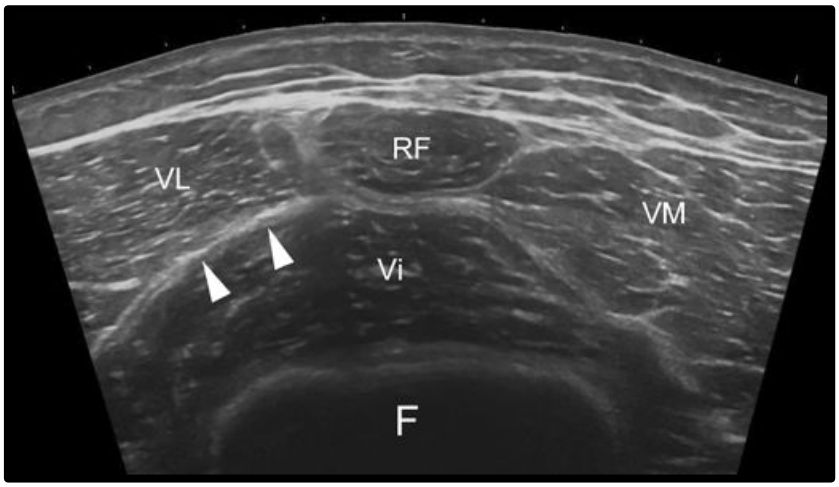

Fig. 4. Extended-field-of- view US scan showing thigh muscles and fasciae (arrowheads) appearance. RF, rectus femoris; VL, vastus lateralis; VM, vastus medialis; Vi, vastus intermedius; F, femur

In **short axis**, muscle tissue appears as dots and short lines producing a “starry sky” appearance (Fig.5).

In **longitudinal section**, the hyperechoic structures, represented by fibroadipose

septa, appear as parallel lines that gives rise to fusiform or pennate appearance (semipennate, unipennate, bipennate, multipennate).

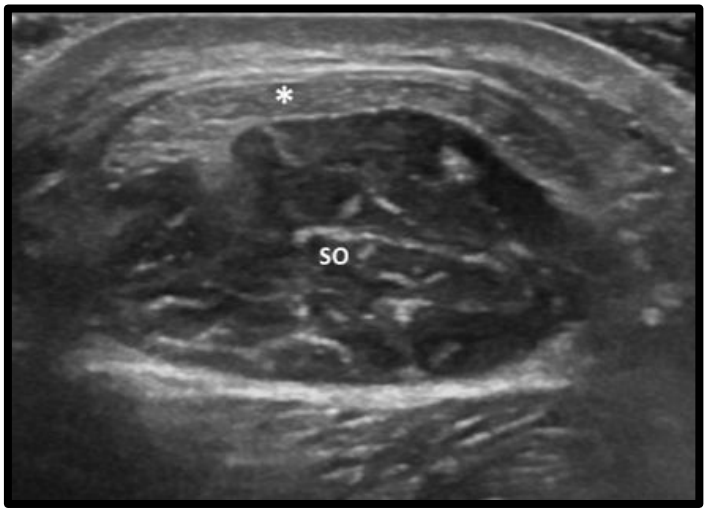

Fig. 5. US scan of the posterior leg showing soleus muscle (SO) internal architecture and, superficially, the forming Achille's tendon (*).

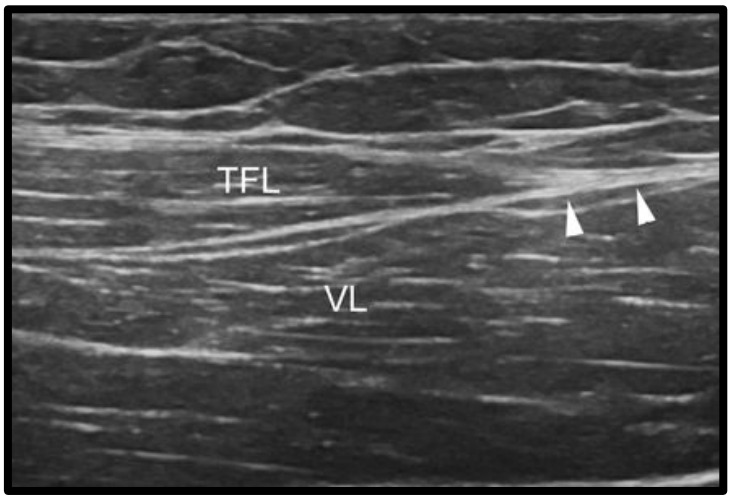

Fig. 6. US scan of the thigh showing the tensor fasciae latae muscle (TFL) and its aponeurosis (arrowheads). VL, vastus lateralis muscle.

In normal subjects the *epimysium* surrounding the muscle appears as a highly reflective structure; the bone, if visualized, appear as a bright echo, representing the cortex, with an anechoic bone shadow (Silvestri 2015).

The intramuscular tendon and the aponeurosis appears as highly hyperechoic linear structures within the muscle; the musculotendinous junction, which varies in size from muscle to muscle, is seen as a hyperechoic fibrillar structure merging with the muscle belly (Fig. 6 and Fig. 7). The fascia appears as a brightly echogenic fibrillar structure that delineates the muscle from subcutaneous tissue and it is very important landmark in order to distinguish the examined muscle from the adjacent ones.

Structure and appearance of skeletal muscles changes with ageing. In addition to age-related muscle mass reduction, muscle quality changes include increased adipose tissue accumulation and water content within muscle that appear highly hyperechoic. Muscle disuse results in altered composition and increased intramuscular fat accumulation. This condition is accompanied by a severe loss of muscle strength.

The examiner should pay attention to evaluate muscles with a correct angle of incidence of the US beam to avoid **anisotropy** artefacts**.** When the US beam is not perpendicular, the muscle shows a loss of echogenicity in structure (Fig. 8).

Because muscle tears and hematomas may appear hypoechoic, it is important to continually move or angle the transducer to prevent anisotropy as the cause of focal hypoechogenicity.

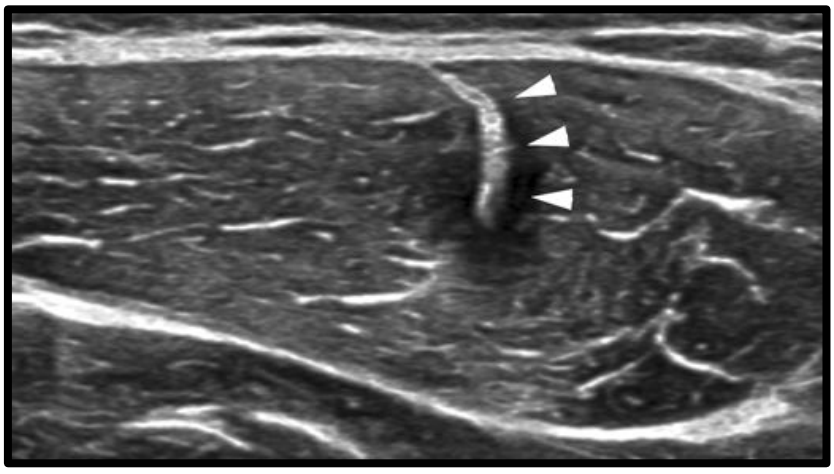

Fig. 7. US transverse scan of the rectus femoris muscle showing tendon appearance (arrowheads).

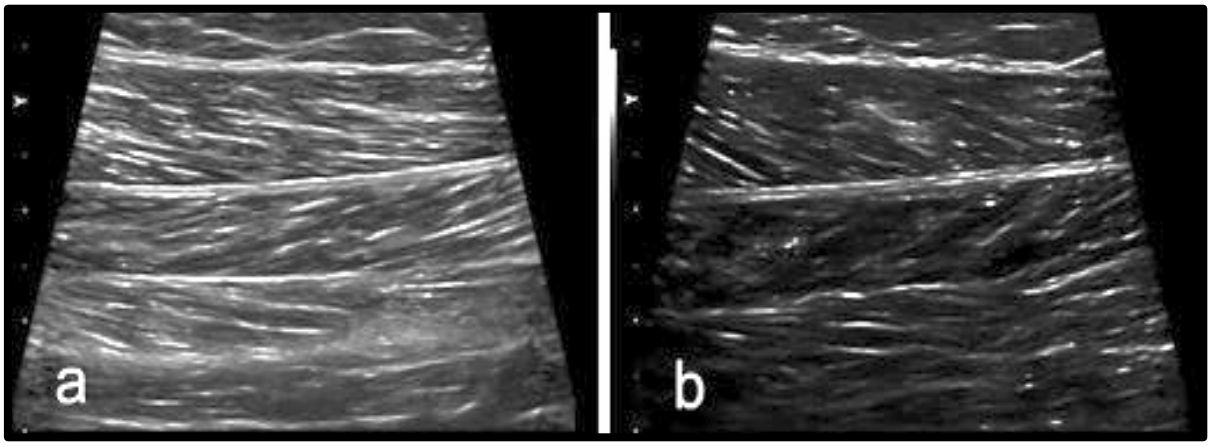

Fig. 8. US scan of medial gastrocnemius muscle showing correct insonation (**a**) and anisotropy artifacts (**b**).

2. Sonoelastography

Sonoelastography (SEL) is a recently developed imaging technique which allows for qualitative visual or quantitative measurements of the mechanical properties of tissues. It is based on the principle for which, applying an extrinsic (mechanical or physical) stress, it is possible to induce changes in a determined tissue, depending on the elastic properties of the tissue itself; hence, qualitative and/or quantitative measurements of the elastic changes induced through the tissue could be obtained, usually by mean of an ultrasound transducer in clinical practice. The recent diffusion of SEL into commercially available ultrasound systems has promoted the development of many studies regarding the potential clinical applications of this technique in different clinical fields (Bamber 2013, Barr 2015, Sigrist 2017, Tang 2015) and, in particular, in the musculoskeletal system (Lehaoux 2020, Brandenburg 2016, Sconfienza 2014, Eby 2013, Klauser 2014).

2.1 Elasticity: basics principles

The elasticity of a material represents its tendency to resume its original shape and size after being subjected to a deforming force or stress. Fluids resist a change in volume but not in shape: they have only ‘volume elasticity’. Solids instead resist changes in volume and shape: they present rigidity or ‘shear elasticity’, as well as volume elasticity. Viscoelastic fuids also exhibit elasticity in certain conditions (Askeland 2006.).

It is essential that the terms stress and strain be defined because the elasticity of a material is described in terms of a stress-strain relation: the ‘strain’ is the relative deformation in volume or shape, produced by a force per unit area (called ‘stress’).

For a homogeneous isotropic solid, the ratio of stress-strain is a constant, called the 'modulus of elasticity'. A modulus measures the amount of force per unit area (stress) needed to achieve a given amount of deformation and usually is expressed in units of Pa. A higher modulus typically indicates that the material is harder to deform (Meriam 2012).

Three moduli are commonly used to define elasticity:

- *Young's modulus* (*E*) represents longitudinal elasticity and is defined by the ratio between the stress and the strain. Young modulus $E = S/e$.
- *Shear or torsion modulus* (*G*) represents transverse elasticity.
- Bulk or volume modulus (*K*) represents volume elasticity.

A stress determines two types of mechanical waves in the tissue:

1. *Compression wave* that compresses tissue little by little, inducing a displacement parallel to the propagation direction

2. *Shear wave* that is responsible of a slip of different tissue layers, relative to each other, inducing a displacement perpendicular to the wave propagation direction

The ultrasound elastography quantitative techniques do not directly measure the Young's modulus but the speed *V* of shear wave propagation.

The velocity *V* of the shear wave is related to shear modulus μ (shear):

$$\mu = rV^2 \text{ with } r = \text{tissue density}$$

The shear modulus μ is itself connected to the elastic modulus:

$$E = 3\,\mu$$

The measurement of the shear wave propagation velocity *V* (in m/s) allows to assess

the elastic modulus E according to the formula:

$$E = 3\mathrm{r}V^2$$

For computations, the tissue density is assumed to be constant and equal to 1000 kilograms per square mm.

The shear modulus describes the response to shear forces, Young's modulus describes the response to linear stress (tensile stress) and bulk modulus represents the response (in all directions) to uniform compression; it is usual for values of shear and Young's modulus to be reported in the studies regarding the investigation of elastic properties of tissues by means of ultrasound (Lerner 1990).

So the aim of elastography is to assess tissue stiffness based on three steps:

1. Excitation: transmission of stress in a tissue

2. Acquisition: recording the signal induced by the tissue deformation due to the stress (RF or B-mode data)

3. Analysis: analysis of tissue strain induced by the propagation of the stress

Human body has a mechanical behaviour similar to a soft homogeneous and isotropic linear elastic material.

2.2 Modalities

There are several elastographic techniques which can be classified based on the temporal characteristics of the excitation, the excitation source, and the method used to detect tissue motion.

2.2.1 Excitation Frequency

Elasticity imaging techniques can generally be classified by the excitation frequency into two categories.

1. Static Excitation: the excitation is applied slowly to allow tissue deformation to reach a steady-state. One of the earliest works to adopt this approach was Ophir et al. in 1991. In that study, tissue was imaged before and after step-wise compression using ultrasound, and images of strain, or 'elastograms', were obtained from tissue displacement. Areas of low strain correspond to hard regions, and high strain to soft regions. Thus, strain images are capable of displaying relative differences in stiffness. This approach has been used for applications such as tumor detection, characterization of vascular plaques, and imaging thermally ablated tissue. Today, static elastography is available on most commercial ultrasound systems. Typically, the operator applies compression on the tissue directly using the imaging transducer. The main drawback of static elastography is that it does not allow quantification of stiffness unless the distribution of applied stress within the tissue is known. Since this is usually not available in practice, it is a non-quantitative technique.

2. Dynamic Excitation: the excitation applied is of short duration (transient) or harmonically oscillating at high frequency. The tissue response in this case is governed by the wave equation. Under simplifying assumptions, the speed of wave propagation in tissue can be directly related to its stiffness. This can be exploited by dynamic elasticity imaging techniques to quantitatively measure the stiffness of

tissue. These methods have been investigated for quantifying the stiffness of various types of tissue, including liver, breast, cardiac, skeletal muscle, artery, kidney, cornea, and brain. Commercial implementations of elasticity imaging using dynamic excitation include FibroScan (Echosens, Paris, France), Virtual TouchTM tissue quantification (Siemens Healthcare, Ultrasound Business Unit, Mountain View, CA, USA), Aixplorer MultiWaveTM Ultrasound System (SuperSonic Imagine, Aix-en-Provence, France) and MR-Touch (GE Healthcare, Buckinghamshire, UK). While dynamic excitation methods allow a quantitative measure of stiffness to be obtained, images formed using wave speed measurements in general have low spatial resolution, and can be susceptible to artifacts in heterogeneous media.

2.2.2 Excitation Source

Three types of mechanical excitation have been used in elasticity imaging.

1. Mechanical actuators: these can be applied to the skin surface to deform the tissue underneath. They can be simple devices, such as plates or the imaging transducer for applying a static compression, or punches for exciting transient wave propagation. Vibration devices offering precise frequency control can be used for dynamic excitation. Interstitial devices, such as intravascular balloons for inducing strains in arteries, have also been used. In general, the amplitude of displacements generated by mechanical actuators applied external to the body in deep lying tissue can be limited by body habitus (obesity and ascites). In addition, wave propagation in tissue is often induced through mode-conversion at the boundary of structures, which can lead to complicated wave fields and makes the reconstruction of elastic parameters a challenging task.

2. Acoustic radiation force: ARF generated by ultrasound can be used to provide mechanical excitation directly to the focal region of an acoustic beam. This allows localized mechanical energy to be delivered directly to deep lying tissue and possibly

avoid interference from intervening fat layers, ascites, or boundaries of surrounding structures. It is attractive for use in ultrasound-based elasticity imaging, as the same transducer can be used for both excitation and imaging. However, significant displacements can only be induced axially along the beamline direction and are small (on the order of microns from conventional diagnostic ultrasound transducers). ARF is predominantly used for dynamic excitation, but can also be used to apply steady-state excitation for short durations (typically milliseconds) (Nightingale 2011).

3. Physiological motion: these methods utilize motion due to respiration, arterial pressure, cardiac, or other muscle activity to provide excitation. These sources have been used to derive elasticity information in arteries, skeletal muscle, and myocardium. Physiological motion can produce appreciable deformation at remote regions inside the body. However, external control of this source of excitation is usually not possible.

2.2.3 Detection Methods

The main methods used for detecting tissue deformation in elasticity imaging are:

1. Ultrasound The first non-invasive measurements of tissue stiffness were made using ultrasound. These early works took advantage of the real-time imaging capabilities of ultrasound and available Doppler processing techniques for detecting tissue motion. Today, it remains the most widely used imaging modality for elasticity imaging, due to short acquisition times (within seconds), portability, low cost, and its ability to also provide mechanical excitation with ARF. However, conventional ultrasound is only able to provide 2D cross-sectional images of the anatomy, and has limited sensitivity to displacements perpendicular to the beam direction, which restricts its ability to fully characterize tissue deformation.

2. Magnetic resonance (MR) Elasticity imaging using MR is often referred to as

magnetic resonance elastography (MRE). It was first proposed by Muthupillai et al. in 1995. This method of detection can be used to image deformation from quasi-static compression, or combined with external vibrators to image wave propagation. Recently, ARF induced tissue deformation has also been imaged using MR. MR has the advantage of being a 3D imaging modality and has the capability to measure displacement fields with equal sensitivity in any direction. However, the long acquisition time required (on the order of minutes) means that most MRE studies are limited to data from a single 2D plane of the anatomy.

2.2.4 Sonoelastography in clinical practice

In clinical practice, among different imaging methods, elastography has emerged in the 90s to provide an estimation of tissue elasticity (Ophir 1991, Lerner 1990). Static and quasi-static elastography were first used to estimate the strain of the muscle qualitatively. Since they offer little advantage, another generation called dynamic elastography, based on propagation of shear waves, emerged (Altahhan 2016). It uses an acoustic radiation force to create and propagate a shear wave offering a quantifiable spatial representation of viscoelastic characteristics of soft tissue (Shiina 2015).

Resuming, two main types of sonoelastography have become established in clinical practice:

• *Strain elastography*: it is also described as ‘quasi-static elastography’, ‘compression elastography’ and ‘real-time elastography’. The stress is applied by repeated manual compression of the transducer, and the amount of tissue deformation (strain) relative to the surrounding normal tissue is measured, usually with a tracking algorithm working on the radio frequency data. The resulting data can then be used to form an image that is coded in colour or greyscale to show the pattern of strain, which is inversely related to tissue stiffness and can be assessed subjectively. These are

qualitative data; however, regions of interest (ROIs) can be positioned over target areas in the screen in order to obtain semi-quantitative analysis (Fig. 9).

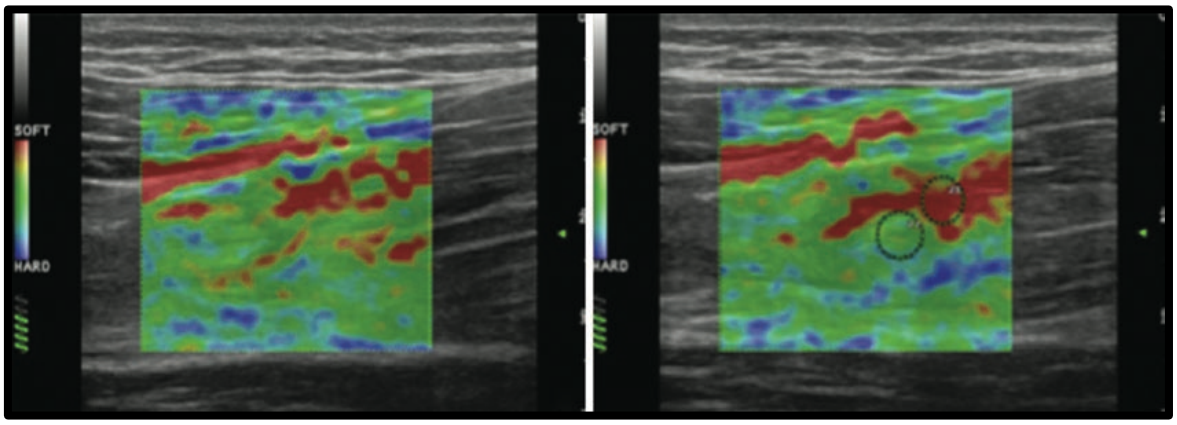

Fig. 9. Strain elastography. (**a**) Qualitative analysis: the modulus of elasticity of the soft tissue scanned in the B-mode image is represented by a superimposed colour-coded map in which (in this case) the lower values are depicted in red and the higher ones in blue; (**b**) it shows the possibility to perform also a semi-quantitative analysis of the strain elastogram with placement of two ROIs in order to take definite measurements of the Young's modulus of elasticity of the targeted tissue. The green-coloured spring-shaped gure shown in the left bottom of both the elastograms indicates that the pressure the operator performed with the transducer was appropriate to produce an adequate stress to get the elastogram.

• *Shear wave elastography*: it is a very potential technique for the noninvasive quantification of tissue stiffness. Shear waves in the body can be induced by various methods, including physiological motion, external mechanical excitation or acoustic radiation force (by a focused ultrasound beam). Shear waves are transverse, they are rapidly attenuated by tissue, they travel much more slowly (between 1 and 10 m/s) and they are not supported by liquids of low viscosity. Using a real-time imaging modality such as ultrasound (but also magnetic resonance), the underlying tissue stiffness can be estimated measuring the produced shear wave speeds. Their speed is commonly expressed in m/s; it is closely related to the modulus of elasticity of the

tissue, and there is a simplified formula for converting between the shear wave speed and the elastic modulus of the tissue to locally quantify its stiffness in kiloPascals (kPa). In contrast to strain elastography, this technique allows for the performance of quantitative analysis of the tissue stiffness (Fig.10).

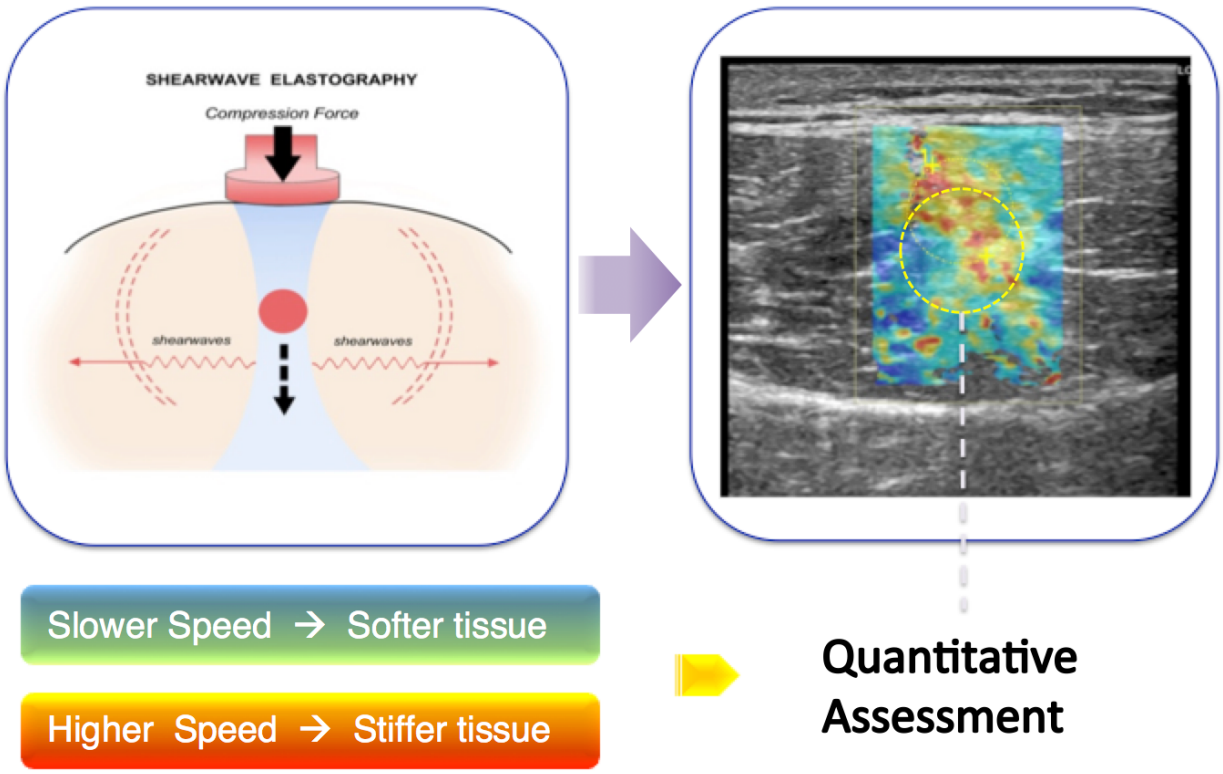

Fig. 10. Shear wave elastography. The focused US beam pushed by the US probe generates shear waves into the target tissue (left); their velocities are detected by the same transducer and represented on the B-mode image (right) by a superimposed colour-coded map in which (in this case) the lower values are depicted in blue and the higher ones in red, giving a quantitative analysis of tissutal stiffness (higher speeds in stiffer tissues and viceversa).

There are some variations of this method in clinical practice, depending on the difference in the modality of stress application:

– *Transient elastography* (TE): it is a system developed and commonly used for liver fibrosis assessment, in which a mechanical piston within an ultrasound transducer is used to apply a push to the skin over an intercostal space. The speed of the produced shear waves into the liver, along the direction of the ultrasound beam, is measured in a way similar to M-mode (Tang 2015).

– *Acoustic radiation force imaging (ARFI)*: in this technique, a focused ultrasound 'pushing' beam (with intensity below the threshold for bio-effects) is used to induce tiny displacements in soft tissue along its direction and generate orthogonal shear waves that propagate sideways in tissue. The shear wave speed or amplitude is detected by conventional ultrasound using tracking algorithms and is used to quantify the underlying tissue stiffness.

Shear wave speed measurement could be made by a single small measurement box positioned by the operator within the tissue adjacent to the pushing beam and/or could be extended to sequential multiple pushing and measurement points in order to construct a colour-coded map of the shear wave speed, which is also quantitative with positionable ROIs. ARFI images represent the spatial distribution of tissue stiffness (Hoyt 2008).

– *Supersonic shear imaging (SSI):* it is a similar system which uses multiple acoustic radiation force impulses focused at different depths to create an extended cylindrical wavefront (Bercoff 2004). These excitations are applied supersonically so that the shear waves generated from different depths constructively interfere adding each other's and dedicated ultrasound transducers could detect and measure them (Gennisson 2010).

An overview of the different elastographic techniques is shown in Tab 2.

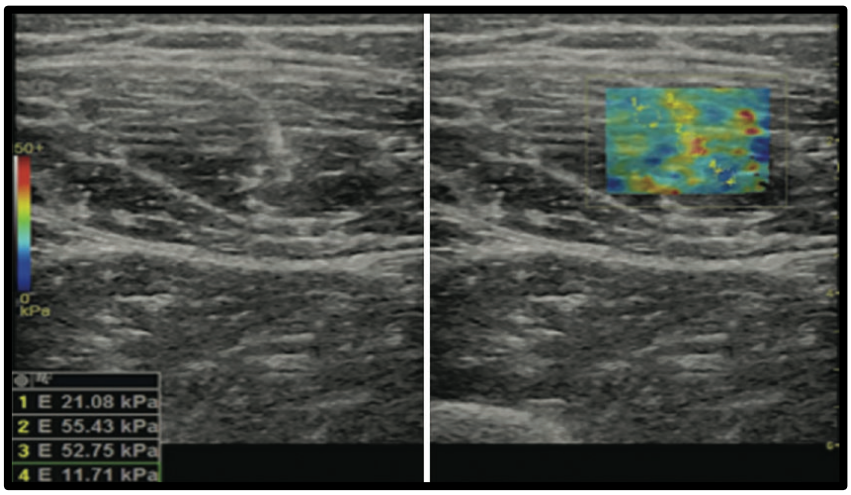

Fig. 11. Shear wave elastography of rectus femoris muscle: after the generation of the 'pushing' beam by the transducer, the values of the shear modulus in the targeted area are represented by mean of a colour-coded map set as represented by the coloured bar on the left of the screen. It is possible to get also a quantitative analysis of the investigated tissue by placing some ROIs (with modifiable dimensions) over the map and get the corresponding value at the left bottom angle of the screen. Note that, on the right elastographic map, the stiffer areas in the centre of the map correspond to the central rectus femoris aponeurosis.

Table II. The technical characteristics of the different elastographic methods.

	Quasi-static	**Dynamic**		
Method	*Strain imaging*	*ARFI*	*Transient elastography*	*SWE*
Excitation mode	Mechanical (external compression) or physiological	Ultrasonic (radiation force)	Mechanical (pulse by an external vibrator)	Ultrasonic (radiation force)
Stress application	Surface or internal structure	Different depths	Surface	Different depths
Involved modulus	Young	Shear	Shear	Shear
Measured parameters	Displacement → strain	Shear wave velocity	Shear wave velocity	Shear wave velocity
Visualization	Temporal strain map	One image	One measure (no image)	Temporal images (several/s)
Quantification	No	Yes	Yes	Yes

3. Pathophysiology of spasticity

Spasticity is a stretch reflex disorder, manifested clinically as an increase in muscle tone that becomes more apparent with more rapid stretching movement. It is a common consequence of lesions that damage upper motor neurons causing upper motor neuron syndrome (UMNS).

3.1. Definition and Clinical Features

The core feature of spasticity is the exaggeration of stretch reflexes. The result is the velocity-dependent increase in resistance of a passively stretched muscle or muscle group. In 1980, Lance published this frequently cited definition: “Spasticity is a motor disorder characterised by a velocity-dependent increase in tonic stretch reflexes (muscle tone) with exaggerated tendon jerks, resulting from hyperexcitability of the stretch reflex, as one component of the upper motoneuron syndrome” (Lance 1980). This definition emphasizes the fact that spasticity is just one component of UMNS.

Besides the dependence from velocity, spasticity is also a length-dependent phenomenon. In the quadriceps, spasticity is greater when the muscle is short than when it is long. This is probably one of the mechanisms underlying the so-called clasp knife phenomenon. On the contrary, in the flexor muscles of the upper limb and in the ankle extensors (triceps surae), spasticity is greater when the muscle is long.

Spasticity is more often found in the flexor muscles of the upper limb (fingers, wrist, and elbow flexors) and in the extensor muscles of the lower limb (knee and ankle extensors). However, there are several exceptions.

3.2 Stretch Reflex and Muscle Tone in Healthy Subjects

In healthy subjects, stretch reflexes are mediated by excitatory connections between Ia afferent fibers from muscle spindles and alpha-motoneurons innervating the same muscles from which they arise. Passive stretch of the muscle excites the muscle spindles, leading Ia fibers to discharge and send inputs to the alpha-motoneurons through mainly monosynaptic, but also oligosynaptic pathways. The alpha-motoneurons in turn send an efferent impulse to the muscle, causing it to contract. Surface EMG recordings in a normal subject at rest clearly show that passive muscle stretches, performed at the velocities used in the clinical practice to assess muscle tone, do not produce any reflex contraction of the stretched muscle. For instance, recording the EMG of elbow flexors during imposed elbow extension, no stretch reflex appears in the biceps when the passive displacement occurs at the velocities usually used during the clinical examination of muscle tone (60 –180 per second). It is only above 200 per second that a stretch reflex can be usually seen. Therefore, stretch reflex is not the cause of the muscle tone in healthy subjects. The muscle tone in healthy subjects is completely due to biomechanical factors (Thillmann 1991).

3.3 Muscle Tone in Patients with Spasticity: The Exaggerated Stretch Reflex

Differently from healthy subjects, in patients with spasticity evaluated at rest (completely relaxed), a positive linear correlation between EMG activity of the stretched muscle and stretch velocity was found using a range of displacement velocities similar to that used in the clinical practice to evaluate the muscle tone. When the passive stretch is slow, the stretch reflex tends to be small (low amplitude) and the tone may be perceived relatively normal or just increased. When the muscle is stretched faster, stretch reflex increases and the examiner detects an increase in muscle tone. Therefore, spasticity is due to an exaggerated stretch reflex (Sheean 2002).

Although spasticity is velocity-dependent, surface EMG recordings show that in many cases if the stretch is maintained (velocity = 0), the muscle still keeps contracting, at least for a time. So, although spasticity is considered classically dynamic, there is also an isometric tonic muscle contraction after the stretch reflex elicited in a dynamic condition (Trompetto 2014).

3.4 Soft Tissue Changes: Intrinsic Hypertonia

Spasticity is responsible for the velocity-dependence of muscle hypertonia in patients with UMNS. However, it must be stressed that in such patients muscle hypertonia is a complex phenomenon, where spasticity represents only one aspect. Hypertonia in patients with UMNS, therefore, can be divided into two components: hypertonia mediated by the stretch reflex, which corresponds to spasticity, and hypertonia due to muscle contracture, which is often referred as non-reflex hypertonia or intrinsic hypertonia. In contrast to spasticity, in intrinsic hypertonia resistance to passive displacements is not related to the velocity of the movement (Marinelli 2017).

3.5 The Exaggeration of Stretch Reflex

Theoretically, the exaggeration of the stretch reflex in patients with spasticity could be produced by two factors. The first is an increased excitability of muscle spindles, for which passive muscle stretch induces a greater activation of spindle afferents with respect to that induced in a normal subject. The second factor is an abnormal processing of sensory inputs from muscle spindles in the spinal cord, leading to an excessive reflex activation of alpha-motoneurons. The velocity-dependence of spasticity can be attributed to the velocity sensitivity of the Ia afferents. However, it has been suggested that II afferent fibers, which are length-dependent, could be responsible for the muscle contraction in isometric conditions often seen after the

dynamic phase of the stretch reflex in patients with spasticity (Sheean 2002).

3.6 Upper Motor Neuron Syndrome: a Complex Picture

After a stroke or a trauma damaging upper motor neurons, weakness and loss of dexterity are immediately apparent. Other signs can be hypotonia and loss (or reduction) of deep tendon reflexes. These signs are known as the negative features of the UMNS. Sometime later, other signs appear, characterised by muscle overactivity: spasticity, increased deep tendon reflexes (also called tendon jerks), clonus, spasms, Babinski sign, positive support reaction, cocontraction, spastic dystonia, and associated reactions. These signs are known as the positive signs of the UMNS (Trompetto 2014).

The hyperexcitability of the stretch reflex produces spasticity, clonus, and the increase of deep tendon reflexes. Increased excitability of the physiological exor withdrawal reflex produces flexor spasms of the lower limbs, commonly seen after spinal cord injuries. On the contrary, cocontraction and associated reactions do not depend on spinal reflexes; therefore, they are efferent phenomena. Also spastic dystonia is thought to depend upon an efferent drive (Marinelli 2017). Cocontraction is the simultaneous contraction of both the agonist and the antagonist muscles around a joint. In healthy subjects, the voluntary output from the motor cortex activates the motoneurons targeting the agonist muscles and, through the Ia interneurons, inhibits those innervating the antagonist muscles (reciprocal inhibition). In the UMNS, cocontraction is due to the loss of reciprocal inhibition during voluntary command. This is likely to be the most disabling form of muscle overactivity in patients with UMNS, as it hampers generation of force or movement. Associated reactions are involuntary movements due to the activation of paretic muscles which occur during voluntary activation of unaffected muscles or during involuntary events such as yawning, sneezing, and coughing (Gracies 2005).

Spastic dystonia refers to the tonic contraction of a muscle or a muscle group when the subject is at rest. It can be described as a relative inability to relax muscles. Spastic dystonia can alter resting posture contributing to the hemiplegic posture: the upper limb is flexed and adducted; the lower limb is extended (Sheean 2009). Although not induced by muscle stretch, spastic dystonia is sensitive to muscle stretch and length. It can be triggered by muscle stretch, even though prolonged stretch can reduce it. The common view is that spastic dystonia is an efferent phenomenon, mediated by an abnormal pattern of supraspinal descending drive. The inability to relax the muscle (i.e., spastic dystonia) is a central feature in spastic patients and is likely to be connected to the prolonged firing of alpha-motoneurons, a well-documented phenomenon in patients with UMNS, possibly having a role in the isometric tonic muscle contraction often seen in spastic patients after the dynamic phase of stretch reflex.

3.8 Supraspinal Influences on the Stretch Reflex

Spasticity is not related to the pyramidal system. It is due to loss or reduction of the inhibitory influences conducted by the dorsal reticulospinal tract and is maintained through the facilitatory influences conducted by the medial reticulospinal tract. Brain lesions cause spasticity when they disrupt the facilitatory corticobulbar fibers, thus leading to the inhibition of the ventromedial reticular formation, from which the dorsal reticulospinal tract takes its origin. Incomplete spinal cord lesions cause spasticity when they destroy the dorsal reticulospinal tract sparing the medial reticulospinal tract. In the complete spinal cord lesion, both the facilitatory and inhibitory influences on the stretch reflex are lost. As all these tracts inhibit the physiological flexor withdrawal reflex, flexor spasms are predominant (Trompetto 2014).

4. Research context

B-mode conventional ultrasonography (US) is widely utilized for musculoskeletal pathology as a first-line approach mainly because of real-time access and the relatively low costs (Klauser, 2014). Sonoelastography is a method that can assess the mechanical properties of soft tissues by US imaging, in particular, a further development of such technique - shear wave elastography (SWE) - provides quantitative evaluation of elastic properties by measuring the propagation velocity distribution of the directional shear waves, produced by an ultrasound pulse (Bamber 2013).

In the past decade, sonoelastography has been established in clinical practice as an effective diagnostic method for the quantitative assessment of liver fibrosis, for breast and thyroid cancer; more recently it has been introduced as a promising diagnostic tool in musculoskeletal pathology to assess muscle and tendon elastic properties related to degeneration, injury and healing (Ryu, 2017, Sconfienza 2014, Creze 2018).

Recently some authors demonstrated good to excellent interobserver reproducibility and intraobserver repeatability in radiologists, validating the feasibility and reliability of ultrasound SWE to assess mechanical properties (stiffness) of skeletal muscle tissue in the upper and lower extremities (Phan 2019, Sarabon 2019, Creze 2018).

Following stroke, paretic limbs may develop muscle hypertonia with a prevalence established in a number of clinical studies ranging from 30% to 80% (Lehoux 2020, Feigin 2017), often related to the appearance of spasticity or spastic dystonia, both related to alpha motor neuron hyperexcitability. Strictly speaking, while spasticity refers to a velocity-dependent muscle hypertonus due to stretch reflex hyperexcitability, spastic dystonia not only causes hypertonus during passive muscle elongations, but also when the muscle is at rest, either before or after muscle

stretching (Marinelli, 2017). Apart from these neural-mediated reflex phenomena, it is well recognized that paretic muscles undergo intrinsic structural changes such as muscle shortening (reduction in number of sarcomeres and fibers size with different distribution) and increased fibrosis (increase in extracellular matrix and collagen concentration with inferior mechanical properties) related to reduced use and immobilization (Trompetto, 2014, Lehoux 2020, Sions 2012, Lee 2019).

Botulinum toxin A (BoNT-A) is considered the first-choice treatment for spasticity affecting a limited number of muscles. It reduces muscle activity by inhibiting acetylcholine release at neuromuscular junction level and is therefore able to reduce neural-mediated muscle hypertonia.
The goals of botulinum toxin treatment include improving limb function, increasing passive/active range of motion (ROM), facilitating better hand hygiene, reducing pain and improving the ability to control limb position (Olvey et al. 2010).

4.1 Rationale

The BoNT-A treatment requires a reliable measure of spasticity to determine the efficacy of the intervention over time. To date, this remains challenging because of the lack of a gold standard (Starky 2005). Although clinical parameters (i.e.: Modified Ashworth Scale - MAS) have been used as clinical assessments before and after treatment, they are subjective and non-quantitative (Sommerfeld 2012). Both conventional surface electromyography (EMG) and intramuscular EMG have been proposed for a quantitative evaluation but they measure only electrical activity of muscles.
In such setting, SWE could gain an important role due to its potential capability to quantitatively assess the contribution of viscoelastic properties to soft tissue stiffness.
Tough, the possibility to match the electromyographic evaluation of spasticity and spastic dystonia before and after botulinum toxin treatment, paralleled with SWE

evaluation, should tell apart neural-mediated and intrinsic muscle stiffness.
Of course, patients with spasticity following stroke are ideal patients for such evaluation since only one side of the body is usually affected, in the context of hemiparesis.

4.2 Study objectives

- Validate elastosonography to assess spastic muscle stiffness: if this method is able to detect stiffness changes before and after botulinum toxin treatment, then it is likely suitable to complement electromyography in the assessment of muscle hypertonia
- Compare the amount of reduction of quantitative measure of muscle hypertonia using SWE and electromyography in order to distinguish the contribution of reflex hypertonia and intrinsic muscle changes by comparing the spastic muscle before and after botulinum toxin treatment (endpoint 1) and with the contralateral unaffected homologue (endpoint 2).

4.3. Population

From September 2018 to December 2019 we prospectively recruited 16 patients (5F; age:59,6±15,2 years, m±SD; range:46-79) affected by spasticity in at least one muscle group of only one side of the body following stroke by at least 3 months. If the patient had already been treated with botulinum toxin, the time interval between the last injection was at least of 4 months.
Inclusion criteria are:
- Age of 18 or more
- Previous ischemic or haemorrhagic stroke occurred at least 3 months before

- Spasticity affecting at least one muscle segment with unaffected contralateral homologue
- Ability to sign the informed consent

Exclusion criteria are:

- Concomitant parkinsonism
- History of lesions affecting the muscle to be evaluated

The institutional review board at I.R.C.C.S. Ospedale Policlinico San Martino approved the study and all patients provided written informed consent before data collection and assessment.

5. Materials and Methods

All recruited patients underwent a neurological examination and assessment of muscle hypertonia using the modified Ashworth scale (MAS).

The MAS score was obtained on all patients by an experienced physician (L.M., neurologist) The MAS is based on one quick stretch and is scored on the following scale (Pandyan 2003, Bohannon 1987):

0 = no increase in muscle tone (i.e., normal)

1 = slight increase in muscle tone, manifested by a catch and release or by minimal resistance at the end of the ROM when the affected part(s) is moved in flexion or extension

1+ = slight increase in muscle tone, manifested by a catch, followed by minimal resistance throughout the remainder (less than half) of the ROM

2 = more marked increase in muscle tone through most of the ROM, but affected part(s) easily moved

3 = considerable increase in muscle tone, passive movement difficult

4 = affected part(s) rigid in flexion or extension.

Among the muscles going to be treated with botulinum toxin following clinical examination, a muscle with MAS > 0 was selected to measure spastic dystonia and spasticity. Muscles characterized by large bulk and reduced distance from the ultrasound transducer (such as biceps brachii muscle) were preferred.

All patients underwent clinical assessment, surface electromyography (sEMG), SWE and B-mode conventional ultrasound assessments. SWE was also performed on the homologue non-paretic contralateral muscle.

The examiners evaluated patients independently and blinded to each other.
MAS, SWE, sEMG and MHS assessments were performed just before botulinum toxin injection (T0) and one month after (T1) with same protocols: such time interval was chosen in relation to the maximum effect of the botulinum toxin after injection.

5.1 Electromyography

Self-adhesive electrodes (Neuroline 700, Ambu A/S, Ballerup, Denmark) were placed at 1cm apart over muscle belly for bipolar recording following SENIAM (Surface Electromyography for Non-Invasive Assessment of Muscles) guidelines (Hermens 1999). Signals were acquired by a BIOAMP LT unit (Vertigo, Genova, Italy) and underwent a 20-500 Hz band-pass filter for offline processing using a custom software running in Labview (National Instrument, Austin TX, USA). Subjects were lying supine on the examination table in a quiet room while attempting to remain relaxed.
1) *Spastic dystonia* was assessed by recording sEMG while the muscle remained in a neutral position, before performing passive limb movements. Each subject entered analysis with the average rectified value (ARV) during a 30s recording.
2) *Spasticity* was assessed in the selected muscle by recording sEMG during 10 passive stretches performed at a reproducible speed, according to a previously validated methodology (Marinelli 2013). The selected muscle was stretched with linear (ramp and hold) passive movements following the pacing provided by an emulated metronome. The beats per minute pace (BPM) was decided for each patient according to the muscle and the amount of spasticity and maintained the same at both time points. Each subject entered analysis with the mean ARV obtained from 10 consecutive stretches before and after botulinum toxin injections.

5.2 Sonoelastography

A LOGIQ E9 ultrasound system equipped with a 9L linear array transducer with Shear Wave Elastography technology (GE Healthcare, General Electric Company, Chicago, Illinois, US) was used to acquire B-mode images, and shear wave elastographic measurements. Such technology uses 'comb-push' excitation source (multiple pushing beams transmitted on the transducer simultaneously in a comb-like pattern), time-interleaved shear wave tracking (data interpolation), directional filters and a time-of-flight algorithm which is used to estimate the local Shear Wave speed at every location in the region of interest.

SWE measurements were performed by a radiologist (A.C.) with 10-year-experience in musculoskeletal ultrasound and 5-year-experience in US-elastography at two time points: prior to BoNT-A intramuscular administration (T0) and 4 weeks after injections (range: 22-32 days). Patients have been placed in the supine position; the patients' arm was held in a non-stretched position with target muscle in a shortened position. Transmission gel was applied, the ultrasound probe was placed on the skin and underlying transverse sections of the muscle belly were scanned. Standard machine settings for acquiring ultrasound data included a maximum image depth of 10 cm, scanning frequency of 7 MHz, single image focus, tissue harmonic imaging and turned off speckle reduction function.

We switched to elastographic mode to measure muscle stiffness, setting shear wave velocity (SWV, m/s) as unit of measurement (Eby 2016). Special attention was paid to placing the transducer lightly on the skin, applying as little pressure as possible on the skin and underlying muscles (in order to prevent any minimal additional pressure on the muscle which could lead to overestimated measures). The region of interest (ROI) for estimating stiffness of the muscle was set between depths of 1.0 and 5.0 cm from the skin and displayed as color-coded SW-velocities (SWV) map on the ultrasound screen. SWVs in the ROI were calculated after a shear wave quality map generated by LOGIQ E9 elastographic software revealed a homogeneous green color

(meaning appropriate push beam and speeds detection). Quantitative SWV values were measured using a rectangular dimension-variable ROI (maximum dimensions: 2 x 2 cm). A total of 10 SWV measurements for each muscle belly were obtained avoiding aponeurosis and thickest intramuscular septa, covering the widest area of muscular fibers (Fig. 12); then, for each muscle, a median velocity (m/s) ± interquartile range (IQR) was provided in order to get a comprehensive estimate of the muscular stiffness. We also performed the same evaluation on the same muscle in a maximum-achievable stretched condition with muscle fibers elongation, while a second operator was keeping the arm of the patient passively extended, as done for EMG measurements.

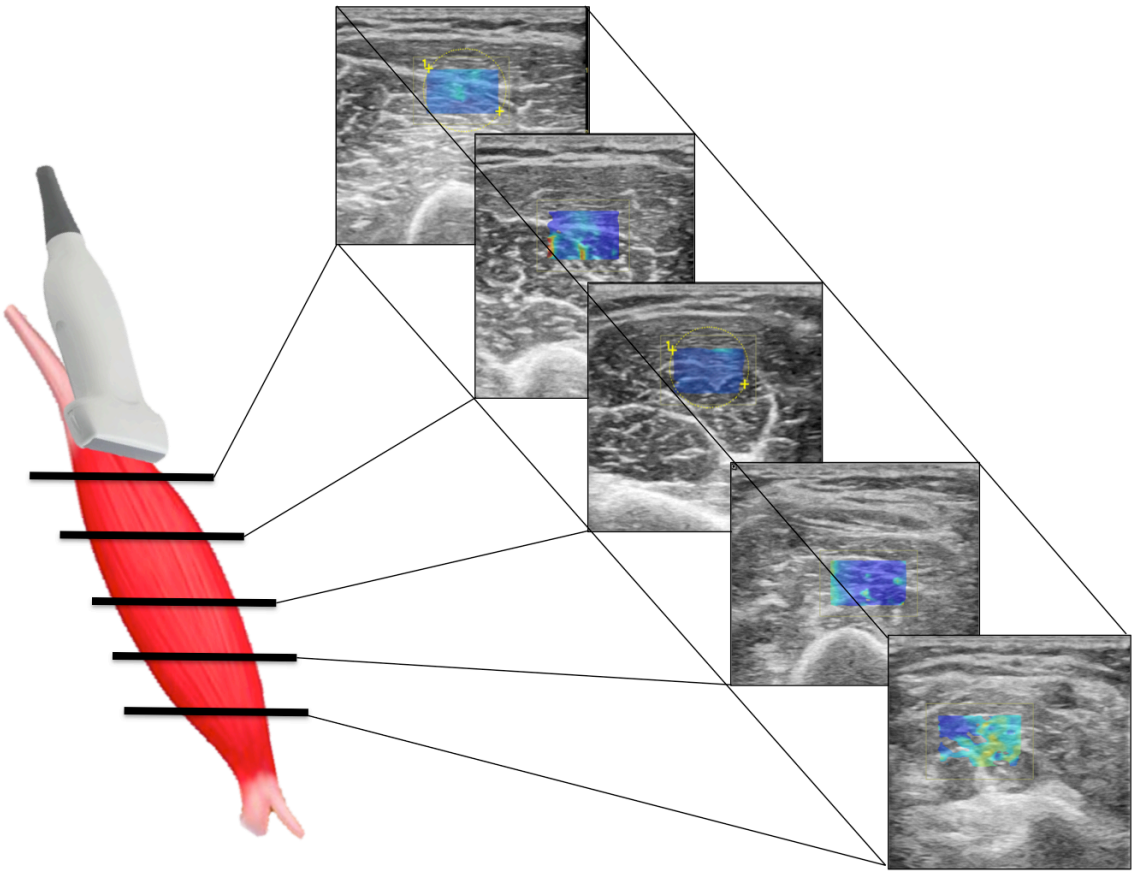

Fig. 12. Scheme illustrating SWE acquisition on short axis of muscular fibers: the transducer is placed on muscular belly performing consecutive transverse scans with the aim of assess the maximum amount of muscle (left); in each scan SW velocities are measured in the positioned ROI generating the relative color-coded elastogram superimposed to the B-mode image (right). A final mean value is then expressed.

Further, analogous SWE measurements were repeated rotating the probe on longitudinal planes of the muscle (as shown in Fig. 13).

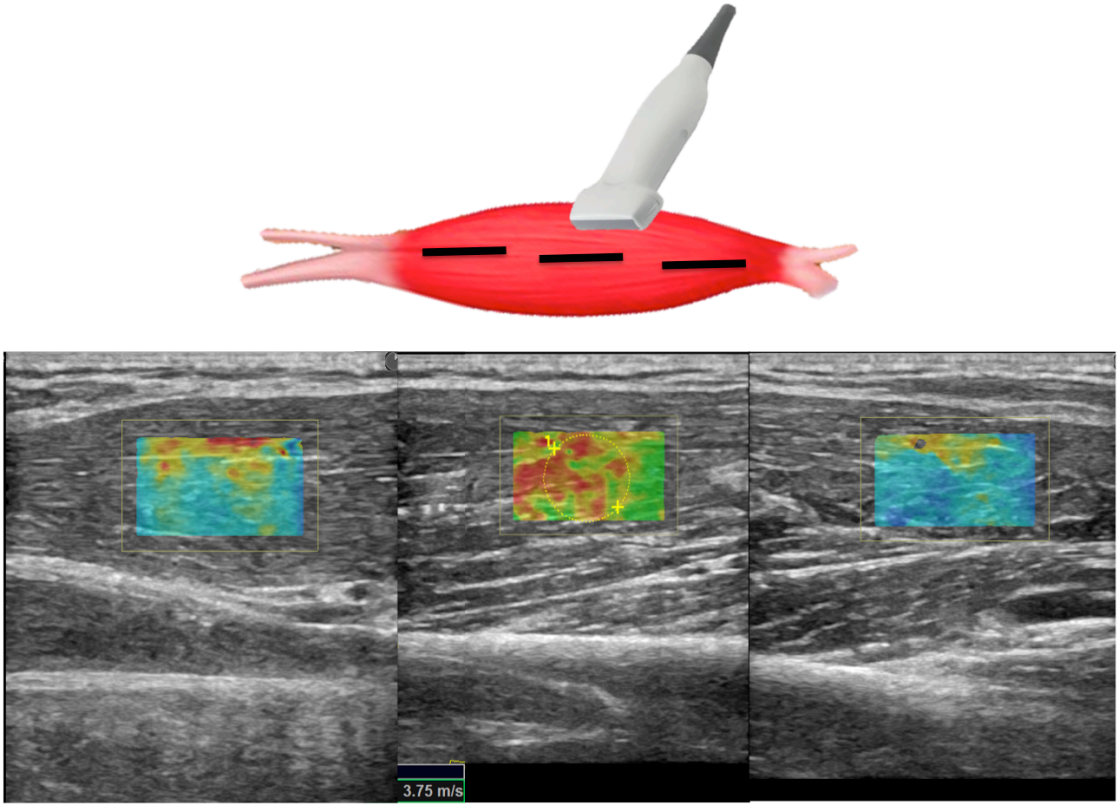

Fig. 13. Scheme illustrating SWE acquisition on long axis of muscular fibers: the transducer is placed on muscular belly performing consecutive longitudinal scans with the aim of assess the maximum amount of muscle (left); in each scan SW velocities are measured in the positioned ROI generating the relative color-coded elastogram superimposed to the B-mode image (right). A final mean value is then expressed.

The same protocol was then performed on the contralateral homologue muscle in order to get differences between paretic and non-paretic side.

Meantime, since the SWE evaluation is provided on the basis of a conventional B-Mode US image, a modified Heckmatt scale (MHS) pattern (Vill 2015) (Fig.14) of

the selected muscle was assessed by the same operator as follows:

1. normal background echogenicity with clearly internal septa;
2. increase in background echogenicity while intramuscular septa are still definable;
3. increase in background echogenicity and less definable septa;
4. increase in background echogenicity without definable septa.

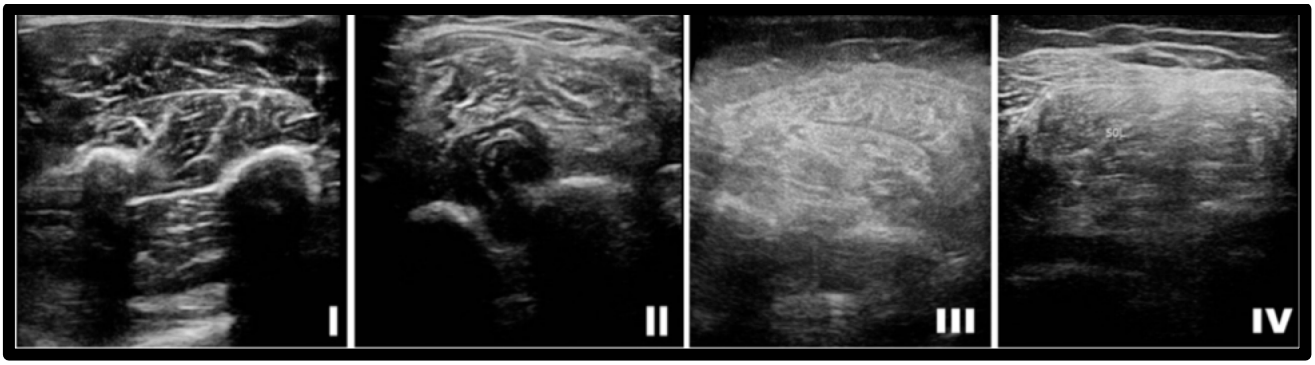

Fig. 14. Modified Heckmatt scale representation. Normal background echogenicity with clearly internal septa (I); increase in background echogenicity while intramuscular septa are still definable (II); 3. increase in background echogenicity and less definable septa (III); increase in background echogenicity without definable septa (IV).

5.3 Botulinum toxin A injection

Botulinum toxin A specifically inhibits acetylcholine release at the neuromuscular junction, thus reducing muscle contraction. Intramuscular injection of BoNT-A is commonly used for the treatment of localized spasticity (Brin 1997).

One hundred-unit vials of incobotulinumtoxinA (Merz Pharma, Frankfurt am Main, Germany) were diluted with 2 ml of preservative-free normal saline. Muscles were injected according to current guidelines according to muscle size and amount of spasticity. Generally, each muscle was injected with 20-100 IU and each patient received no more than 400 IU. A neurologist (L.M.), with more than 10 years of

experience in post-stroke spasticity treatment, performed BoNT-A injections under US-guidance.

5.4 Statistical analysis

Data are expressed as mean±SD. For non-Gaussian distributions data are also reported as medians and interquartile range (IQR, 25%-75%). Statistical analyses were performed using GraphPad Prism v5.0 software (GraphPad Software Inc., La Jolla, CA, USA). Normal distribution of data was assessed by Shapiro Wilk test. Depending on data distribution, paired ANOVA tests for Gaussian and non Gaussian distributed data were performed to evaluate differences among the groups of measurements, using Dunn's or Bonferroni's post-tests for one-way and two-way analyses, respectively. For comparison between two groups of measurements, paired Student's t test or Wilcoxon matched paired test were applied for normal and non-normal distributed data, respectively. Spearman's r was calculated to assess correlation between Heckmatt scale and T0 or T1 measurements; p values <0.05 were considered statistically significant. Effect sizes were calculated as Cohen's d using *effsize* library for R (v3.6.1).

This was a pilot study; we had no preliminary data to estimate the sample size.

6. RESULTS

One of our participant exited the study because of further intervened health problems and another patient was excluded from the study because a concomitant parkinsonism was diagnosed, matching one of our exclusion criteria.
Finally, 14 patients (5F; age: 58,4±14,1 years, m±SD; range:46-78) were included in the study with a total of 28 muscles evaluated. Detailed data are exposed in Tab III.

Patient	Gender	Age	Lesion/affected side of the body	Time since stroke	TargetMuscle
1	M	49	hemorragic/ left	5 aa (2014)	Flexor Digitorum Sup.
2	M	78	ischemic/ right	3 aa (2016)	Brachialis
3	M	46	ischemic/right	7 aa (2012)	Soleus
4	F	48	hemorragic/ right	1 aa (2018)	Gastrocnemius
5	F	57	ischemic/right	6 aa (2013)	Biceps Brachii
6	M	65	hemorragic/ right	3 aa (2016)	Brachialis
7	M	62	ischemic/left	5 aa (2014)	Biceps Brachii
8	F	46	ischemic/ right	14 aa(2005)	Brachialis
9	M	71	ischemic/ right	8 aa (2011)	Gastrocnemius
10	F	42	ischemic/right	3 aa (2016)	Gastrocnemius
11	M	62	ischemic/right	4 aa (2015)	Biceps Brachii
12	M	62	ischemic/ left	4 aa (2015)	Brachialis
13	F	60	ischemic/left	2 aa (2017)	Soleus
14	M	69	ischemic/left	>10 aa (<2012)	Biceps Brachii

Tab. III. Anamnestic features and muscle evaluated of patients included in the study.

6.1 Surface Electromyography

In one subject (#14) a MAS=4 prevented the assessment of spasticity since the elbow joint could not be passively displaced. Average Rectified Value of the EMG signal (ARV) (Hermens, 1999) detected in muscles in neutral position resulted 8.07±8.24 μV (mean±SD) at T0 and 2.65±1.62 μV (mean±SD) at T1; ARV detected during passive extension of muscles resulted 18.13±22.61 μV (mean±SD) at T0 and 7.30±3.70 μV (mean±SD) at T1. Both spastic dystonia and spasticity significantly decreased at T1 after BoNT-A injection (Fig. 15).

.

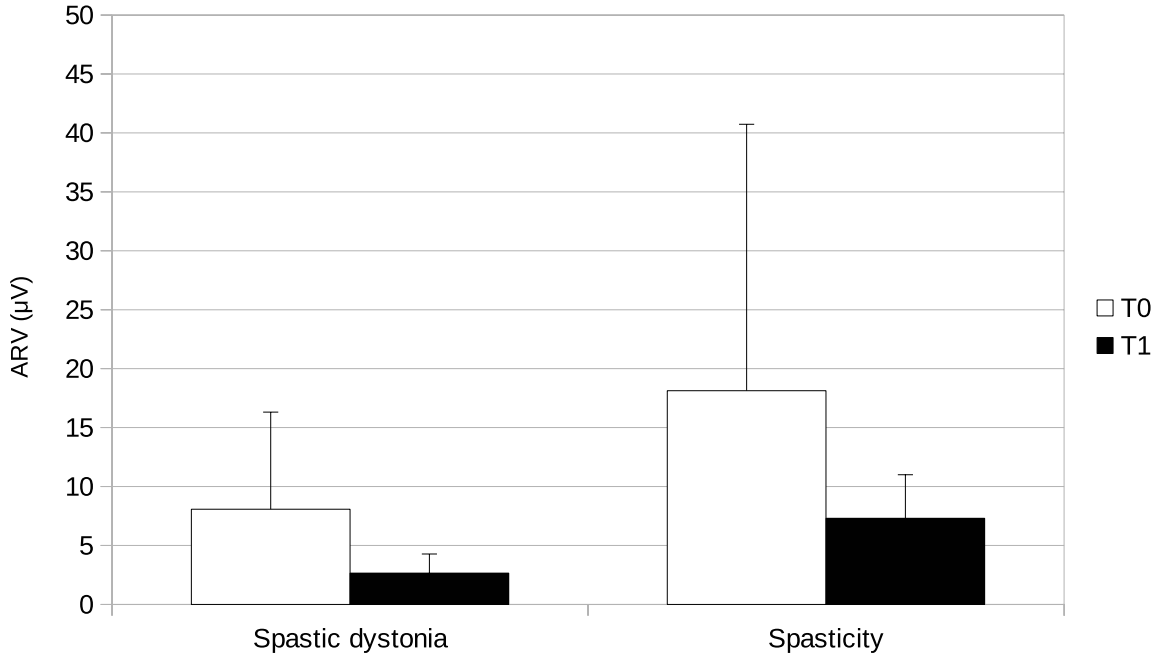

Fig.15 Chart illustrating the electromyographic activity (μV) measured in spastic muscles before (T0) and 4 weeks after (T1) botulinum toxin A injection at muscle relaxation (spastic dystonia) and during passive extension (spasticity).

6.2 Modified Ashworth Scale

MAS values at T0 were 2.32±0.87 (mean±SD); at T1 significantly decreased to 1.79±1.03, mean±SD ($p<0.01$). (Fig. 16). No significant correlation was found among MAS values reduction at T1 (ΔT0-T1) and Δ values of SWE and EMG between the two time points.

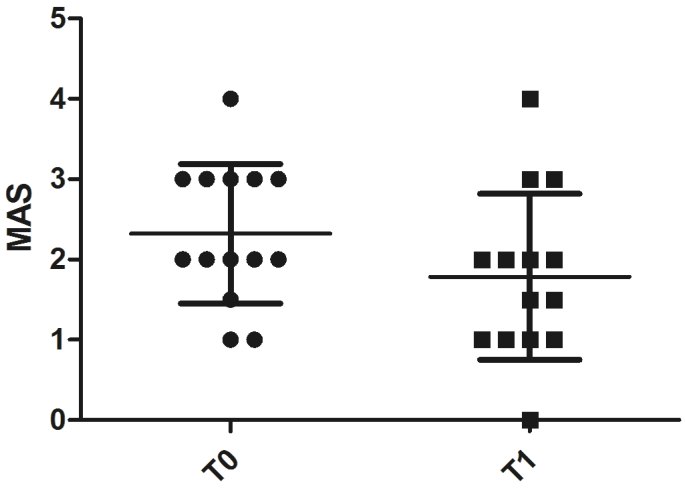

Fig. 16 Chart illustrating the significant difference in MAS scores assessments of spastic muscles before (T0) and 4 weeks after (T1) botulinum toxin A injection.

6.3 Shear Wave Elastography

A total of 224 SWE values resulted considering both time points, subdivided into 8 different groups in relation to the 4 different variables: time point (T0 vs T1), body side (paretic limb vs non-paretic limb), transducer orientation (tranverse vs longitudinal) and muscle condition (stretched vs non-stretched).

Measurements obtained with transverse positioning of the probe, on non-paretic and non-stretched muscle (Group A) resulted 1.98±0.37(mean±SD) at T0 and 1.97±0.38(mean±SD) at T1;

Measurements obtained with longitudinal positioning of the probe, on non-paretic and non-stretched muscle (Group B) resulted 2.88±0.29(mean±SD) at T0 and 2.86±0.29(mean±SD) at T1;

Measurements obtained with transverse positioning of the probe, on non-paretic and stretched muscle (Group C) resulted 2.94±0.26(mean±SD) at T0 and 2.92±0.28(mean±SD) at T1;

Measurements obtained with longitudinal positioning of the probe, on non-paretic and stretched muscle (Group D) resulted 3.47±0.3(mean±SD) at T0 and 3.50±0.34(mean±SD) at T1;

Measurements obtained with transverse positioning of the probe, on paretic and non-stretched muscle (Group Ap) resulted 2.39±0.55(mean±SD) at T0 and 2.34±0.58(mean±SD) at T1;

Measurements obtained with longitudinal positioning of the probe, on paretic and non-stretched muscle (Group Bp) resulted 3.18±0.34(mean±SD) at T0 and 3±0.32(mean±SD) at T1;

Measurements obtained with transverse positioning of the probe, on paretic and stretched muscle (Group Cp) resulted 3.30±0.27(mean±SD) at T0 and 3.29±0.26(mean±SD) at T1;

Measurements obtained with longitudinal positioning of the probe, on paretic and stretched muscle (Group Dp) resulted 3.87±0.44(mean±SD) at T0 and 3.75±0.38(mean±SD) at T1. (Tab.IV)

Overall, SWE measurements on paretic muscles assessed with a longitudinal positioning of the probe showed statistically significant reduction at T1 versus T0 both in non stretched conditions ($p=0.001$) and in stretched conditions ($p=0.0029$) (Fig. 17 and 19).

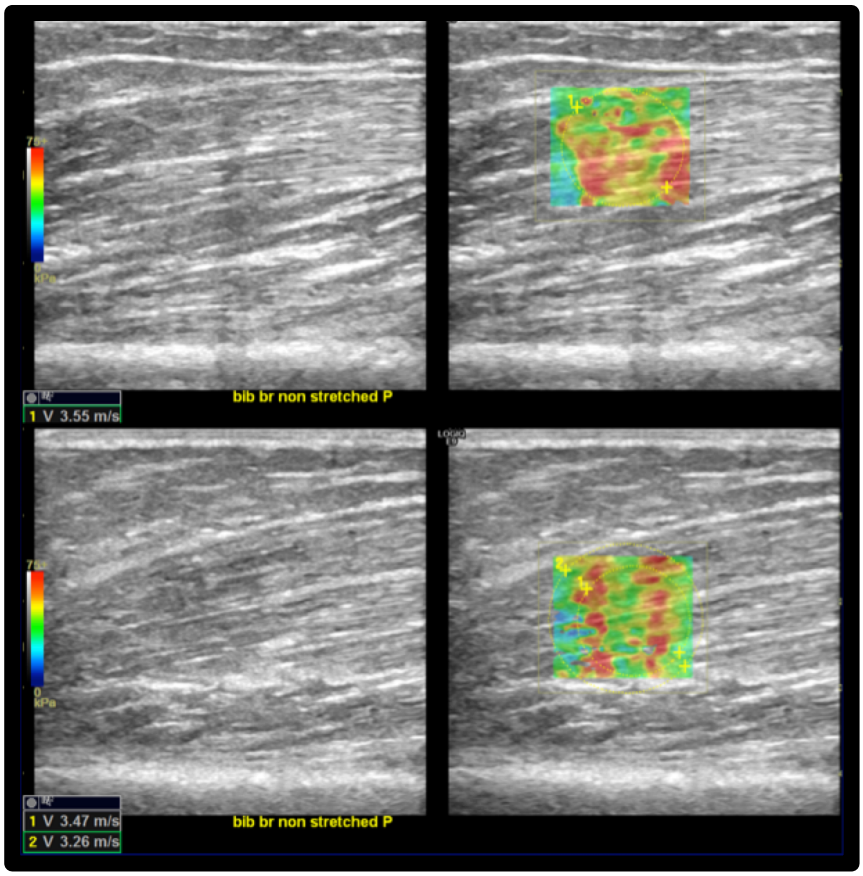

Fig. 17 SWE reduction between T0 and T1. In the upper-right quadrant is illustrated an example of an elastogram (superimposed to the B-mode image) generated by a ROI placed in biceps brachii muscular belly along the direction of the fibers at T0; in the lower right image the same evaluation at T1 shows lower values (lower left corners of the images). Images on the upper- and lower-left quadrant are the respective B-mode conventional US image automatically paired on the screen by the SEL software.

Conversely, SWE assessments with a transverse orientation of the probe did not show a statistically significant reduction between the two time points in stretched conditions ($p=0.66$), and a slighly significant difference in non stretched ones ($p= 0.03$).

Sonoelastographic measurements on non-paretic muscles did not significantly decrease between the two time points, apart from group B ($p=0.04$). (Fig. 20).

All SWE measurements on paretic muscles are sistematically higher than correspective ones on non-paretic muscles ($p<0.01$ for all variables).

Further, SWE measurements obtained in stretched conditions are sistematically higher than measures assessed in non stretched conditions.

SWE measurements obtained with a longitudinal positioning of the transducer are sistematically higher than measures performed with a transverse orientation of the probe ($p<0.01$ for all variables) (Fig. 18).

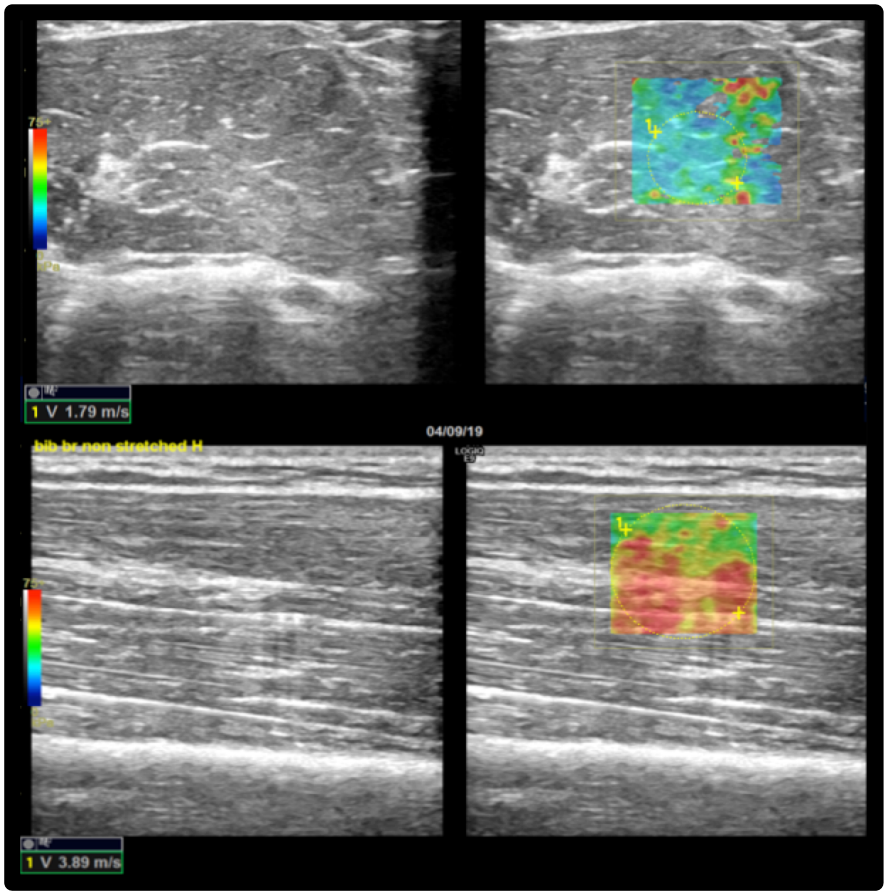

Fig. 18 Example of SWE difference between transverse and longitudinal assessments. In the upper-right quadrant is illustrated an example of an elastogram (superimposed to the B-mode image) generated by a ROI placed in a non-paretic, non-stretched biceps brachii muscular belly across the direction of the fibers; in the lower right image the elastogram generated along the direction of muscular fibers of the same muscle shows higher values expressed both qualitatively with different-coloured map and quantitatively in m/s (lower left corners of the images). Images on the upper- and lower-left quadrant are the respective B-mode conventional US image automatically paired on the screen by the SEL software (transverse US scan in the upper-left quadrant and longitudinal US scan in the lower-left quadrant).

Patient	mHeckmatt Scale	NPnsAxT0	NPnsAxT1	NPnsLoT0	NPnsLoT1	NPsAxT0	NPsAxT1	NPsLoT0	NPsLoT1	PnsAxT0	PnsAxT1	PnsLoT0	PnsLoT1	PsAxT0	PsAxT1	PsLoT0	PsLoT1
1	3	2.56	2.46	3.42	3.37	3.48	3.55	4.35	4.55	3.07	3.17	3.74	3.54	3.68	3.58	4.77	4.65
2	3	2.37	2.49	3.08	3.02	2.92	2.78	3.25	3.34	2.64	2.54	3.39	3.18	3.13	3.17	3.82	3.71
3	3	2.4	2.38	3.21	3.15	3.22	3.24	3.51	3.42	2.94	2.96	3.78	3.49	3.72	3.6	4.17	4.07
4	1	1.55	1.58	2.79	2.71	2.8	2.74	3.2	3.28	1.45	1.34	2.95	2.69	2.82	2.84	3.27	3.36
5	3	2.33	2.4	3.02	3	3.3	3.23	3.44	3.34	2.96	2.88	3.32	3.1	3.4	3.46	3.5	3.45
6	3	1.97	1.9	2.93	2.86	2.82	2.82	3.41	3.5	2.21	2.2	3.24	2.98	3.42	3.31	4.2	4.12
7	2	1.84	1.79	2.55	2.49	2.81	2.77	3.37	3.36	2.3	2.23	2.96	2.74	3.45	3.54	3.85	3.78
8	3	2.28	2.32	3.04	3.08	3.2	3.22	3.64	3.66	2.93	2.95	3.49	3.37	3.35	3.37	4.7	4.2
9	1	1.41	1.39	2.29	2.32	2.7	2.68	3.11	3.12	1.35	1.33	2.97	2.95	2.84	2.73	3.47	3.31
10	2	2.12	2.14	3.05	3.1	3	3.06	3.45	3.43	2.76	2.68	3.3	3.1	3.2	3.32	3.72	3.62
11	2	1.97	1.88	2.9	2.92	2.86	2.8	3.26	3.22	2.56	2.51	3.1	2.97	3.05	3.1	3.58	3.44
12	2	1.58	1.55	2.69	2.63	2.73	2.76	3.5	3.58	2.17	2.07	2.68	2.56	3.27	3.3	3.68	3.61
13	2	1.65	1.68	2.74	2.69	2.6	2.65	3.67	3.69	2.01	1.96	2.83	2.71	3.53	3.41	3.84	3.71
14	2	1.66	1.63	2.67	2.69	2.7	2.64	3.42	3.46	2.07	1.98	2.78	2.59	3.37	3.34	3.67	3.52
MEAN	2.29	1.98	1.97	2.88	2.86	2.94	2.92	3.47	3.50	2.39	2.34	3.18	3.00	3.30	3.29	3.87	3.75
SD	0.73	0.37	0.38	0.29	0.29	0.26	0.28	0.30	0.34	0.55	0.58	0.34	0.32	0.27	0.26	0.44	0.38

Tab. IV SWE and MHS detailed data at T0 and T1 reported as mean±SD. SWE results are classified in columns in relation to the different variables in consideration. (NpnsAx: group A; NpnsLo: group B; NpsAx: group C; NpsLo: group D; PnsAx: group Ap; PnsLo: group Bp; PsAx: group Cp; PsLo: group Dp).

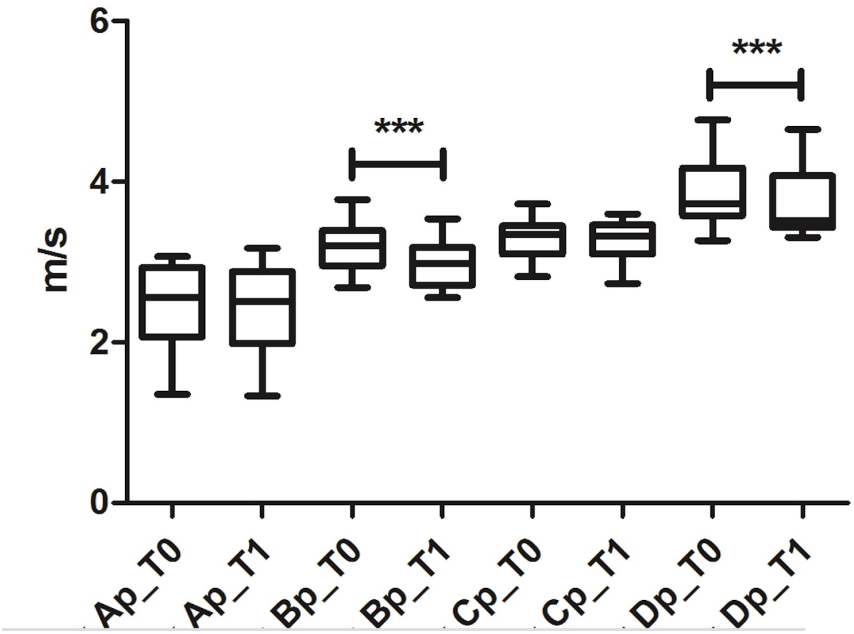

Fig. 19 Chart illustrating SWE velocities (expressed as medians and IQR) assessed in paretic muscles at T0 and T1; significant difference ($p<0.01$) found in longitudinal assessments (group Bp and Dp).

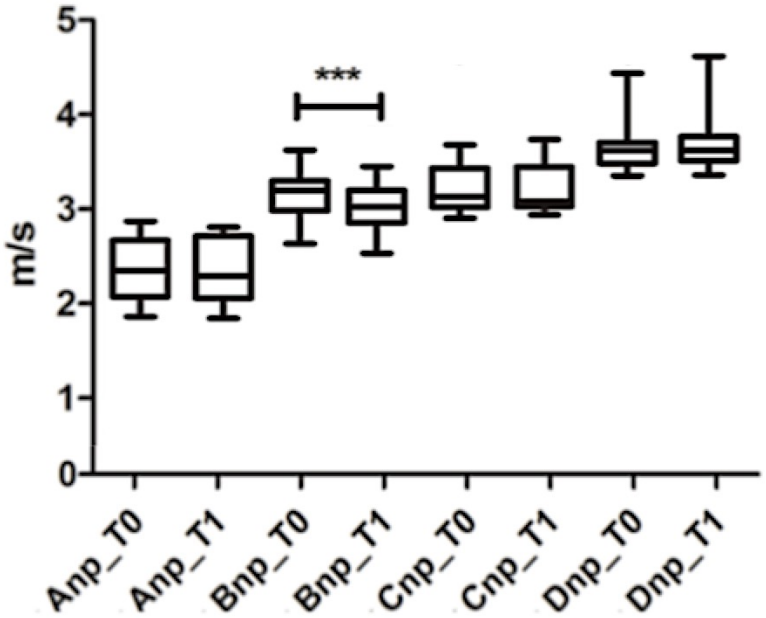

Fig. 20 Chart illustrating SWE velocities (expressed as medians and IQR) assessed in non-paretic muscles at T0 and T1; only a slight significant difference (p:0.04) found in group B.

6.4 Modified Heckmatt Scale

MHS scores (2.29±0.73, mean±SD) did not change between T0 and T1. There was a positive correlation between MHS scores and SWE values: such correlation ranged from moderate to strong (Spearman r: 0.46 - 0.84; results in details in Tab. V) and is significant for every group apart from group D.

	Spearman's r		p-values	
	T0	T1	T0	T1
A	0,8293	0,8458	P<0.0001	P<0.0001
B	0,7292	0,6921	0,0013	0,0042
C	0,699	0,7423	0,0026	0,0015
D	*0,4768*	*0,4653*	*0,0619*	*0,0805*
Ap	0,7492	0,7618	0,0008	0,001
Bp	0,7492	0,7459	0,0008	0,0014
Cp	0,6126	0,6348	0,0117	0,011
Dp	0,7038	0,7625	0,0023	0,0009

Tab. V Correlation between MHS values and different SWE group of measurements: Spearman's r and significance.

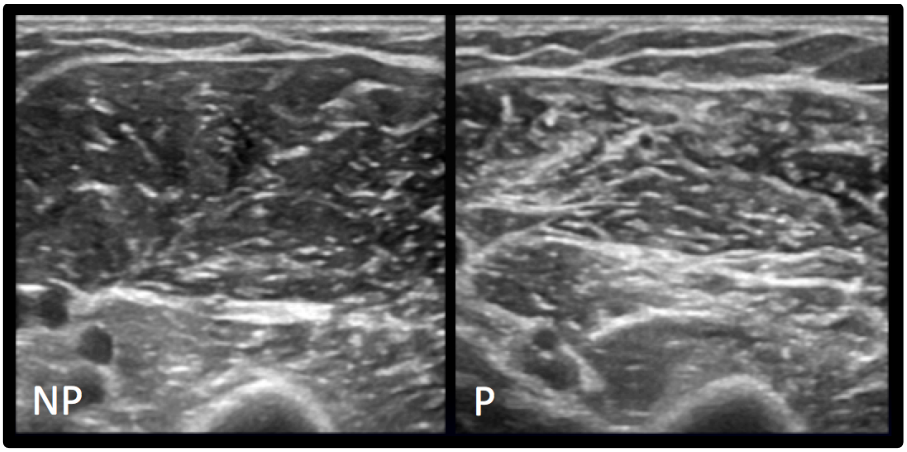

Fig. 21 MHS grade II. Conventional US appearance of biceps brachii and brachial muscles on non-paretic (NP) and paretic side (P) following stroke, as assessed with transverse US scans: on the left image normal US appearance of muscle with regular echogenicity of fibers and normal muscular fibers - intrasmuscular septa differentiation; the right image shows volume reduction of muscle and increase in background echogenicity with intramuscular septa more represented and still definable.

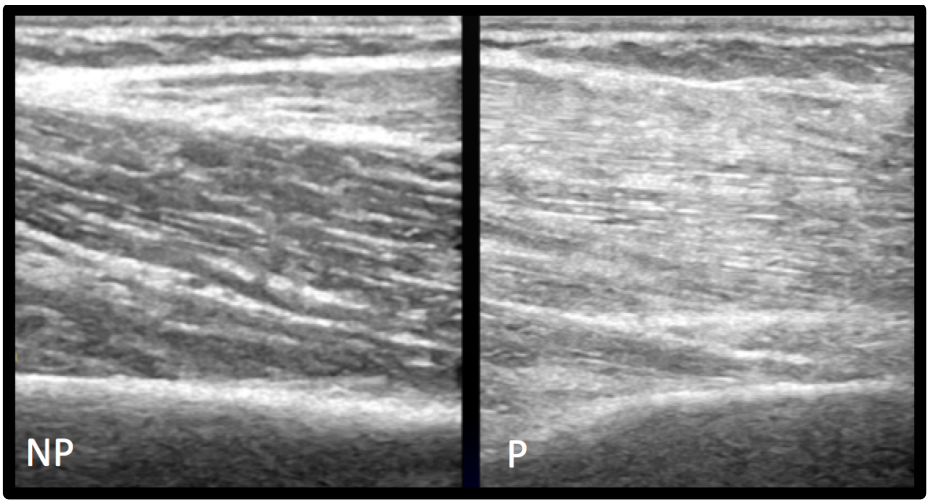

Fig. 22. MHS grade III. Conventional US appearance of biceps brachii and brachial muscles on non-paretic (NP) and paretic side (P) following stroke, as assessed with longitudinal US scans: on the left image normal US appearance of muscle with regular echogenicity of fibers and normal muscular fibers - intrasmuscular septa differentiation; the right image shows volume reduction of muscle and significant increase in background echogenicity with intramuscular septa more represented and less definable.

6.5 Effect size

The effectiveness of botulinum injection on SWE and sEMG measurements, expressed as effect sizes, is reported in tab VI.

Cohen's *d* estimate a larger effect on EMG values than longitudinal SWE ones (either in non stretched and in stretched condition), with narrower 95%CI for SWE measurements.

Cohen's d	Rest	Stretched
SWE	0.543 (CI95: 0.425, 0.660)	0.320 (CI95: 0.166, 0.474)
Elettromiografia	1.084 (CI95: 0.261, 1.907)	0.507 (CI95: -0.073, 1.086)

Tab VI Effect sizes of longitudinal SWE and sEMG related to BoNT-A injection.

6.6 Time since stroke

Poor correlation was found among time since stroke and elastographic, electromyographic and MAS values.

Conversely, good correlation emerged between time since stroke and MHS values (r_s= 0.68472, p= 0.0069).

7. DISCUSSION

Surface electromyography is considered the gold standard for measuring spasticity and spastic dystonia, being the only technique able to record involuntary muscle activity during passive muscle elongations and at rest (Trompetto 2014).
In recent years, many studies (Eby 2016, Gao 2018, Jakuboski 2017, Lee 2019, Le Sant 2018, Mathevon 2018, Wu 2017) used SWE with different approaches and protocols, in order to quantify muscular stiffness related to spasticity.
To my knowledge, this is the first attempt to quantitatively assess the structural and neural-mediated components of spasticity by mean of sEMG and SWE.
Two main observation resulted by this study.

First, SWE, sEMG and MAS were able to detect the effect of BoNT-A on paretic muscles in terms of a significant decrease in their values, as previously demonstrated in several studies (Lehoux 2020).
Following BoNT-A injection, both elastographic and electromyographic measurements decreased because both are affected by neural-mediated stiffness. Such results were expected and should be related to the fact that SWE estimates muscular stiffness measuring its viscoelastic behaviour, hence, is unable to properly differentiate stiffness due to muscle fibrosis or by muscle contraction (two simultaneous phenomena which sum up in spasticity).
Cohen's d values estimated a larger effect size on EMG measurements in respect to longitudinal SWE ones: indirectly, it may be speculated a steeper reduction of electromyographic activity compared to SWE-detected stiffness, which would reflect a reduction in neural-mediated stiffness but not that due to intrinsic muscle changes.
Regarding SWE measurements, significantly ($p<0.01$) decreased values at T1 were limited to the group of measurements obtained with a longitudinal orientation of the probe in respect to the direction of muscular fibers.
Such findings are encouraging because they reflect the physical properties of skeletal

muscle and, moreover, are comparable with results from recently published studies (Creze 2018, Gennisson 2010, Lehoux 2020). Because of the well known physical assumption that skeletal muscle is an anisotropic (orthotropic), non-linearly viscoelastic and deformable tissue, shear waves generated into such tissue propagates in different ways in respect to the orientation of muscular fibers. It may be argued that shear waves which propagate on a transverse axis in respect to the direction of the muscular fibres, encounter a greater number of tissutal interfaces, resulting in more etherogeneous measurements. Conversely, shear waves which propagates along the direction of the muscular fibers could generate more homogeneous measurements.

Further, orthotropic physical properties of skeletal muscle are also responsible for the fact that shear waves travel faster along the direction of the fibers than they do when perpendicular to them, which is another point resulted in the present study and already demonstrated by previous papers (Creze 2018, Dorado 2016, Eby 2016, Miyamoto 2015).

Surface EMG with the proposed protocol, is able to detect the neuro-modulated reflex component of hypertonia as well as the effect induced by BoNT-A injection.

These results were widely expected and and confirm previous published studies (Marinelli 2013).

Also MAS scores consistently decreased after BoNT-A injection, nevertheless, no correlation between MAS values and muscular stiffness as assessed with SWE has been found in this study. This absence of correlation can be probably attributed to the many limitations of MAS because of its inability to distinguish between intrinsic and neural-mediated hypertonus and subjective interpretation of muscle resistance.

Second, SWE showed capability to differentiate paretic from non-paretic muscles.

Statistically significant differences emerged between velocities detected on paretic muscles and respective contralateral ones, in particular SW speeds from paretic muscles were consistently higher.

Such finding was detected both with shortened and passively stretched position of different muscles; in the former condition it may be related to the main contribution of structural (fibrotic involution) changes; in the latter condition spastic dystonia and stretch reflex in paretic muscle should play a pivotal role.

Further, the greater reduction of SW speeds detected at T1 in stretched muscles, in respect to shortened ones, was an expected finding due to the exclusive effect of BoNT-A on hypertonic stretch reflex.

Conversely, in non-paretic muscles SW velocities do not significantly modify between the two time points T0-T1 (apart from a minimum change in group B): this was a crucial finding which indirectly reinforce data resulted from paretic muscles.

The minimum change detected in group B could not be easily explained, it may be argued the development of a 'general' muscular relaxation after BoNT-A injection involving also contralateral muscles possibly related to the reduction of hypertonus and pain on paretic muscle.

Kesikburun in 2015 found that stiffness measured with sonoelastography was increased in the gastrocnemius muscle on the affected side compared to the unaffected side in subjects with unilateral stroke. Some other authors (Gao 2018; Mathevon 2018; Rasool 2018) did not show a significant difference between the paretic and non-paretic limbs; otherwise, they showed difference between limbs and control groups supporting the fact that spastic muscles tend to have greater SW speed than non-spastic ones.

The link between the time of the onset of the stroke and the SW speed values has been shown in three studies (Lee et al., 2015; Lee et al., 2019; Wu et al., 2017).

The lack of correlation resulted in this study between time since stroke and the stiffness of paretic muscle could be probably due to the heterogeneity of stroke's sequelae, age, lifestyles and rehabilitation programs but, mainly, to the fact that spasticity is a multifactorial pathophysiologic process.

Conversely, good correlation emerged between time since stroke and MHS values reflecting involutive structural changes occurring to paretic muscles over time and detectable with conventional US.

Further, MHS values showed positive correlation with SWE measurements reflecting the role of structural involutive changes in muscle architecture in the development of spasticity and its direct connection with viscoelastic properties of paretic muscles.

As expected, MHS scores did not modify between T0 and T1 confirming that BoNT-A has no effect on structural fibrotic changes of paretic muscle, at least after a single injection.

This study had some limitations. The first limit of the study was that SWE measurements were obtained only by one US-experienced operator: ultrasound elastography has the same issues of ultrasonography, which is operator dependent, and, to date it lacks a standardization of the methods (Creze 2018, Eby 2016, Lehoux 2020, Shin 2016). Even if several studies report good reliability of SWE in the assessment of skeletal muscle stiffness (Phan 2019, Sarabon 2019, Creze 2018), giving the technical difficulties SWE requires to be properly performed, less experienced examiners could not achieve the same results. Further, all SWE measurement were conducted with a single US equipment: this could have been a limitation in particular considering that different manufacturers implemented his own algorithms and post-processing calculation to assess mechanical properties quantifying the shear wave speed. Since electromyographic and SWE assessments have been performed in different sessions and environmental conditions, we cannot be sure that patients reached the same level of muscle relaxation/contraction during the two measures: this could have been a further limitation of the study. Last, the number of patients enrolled in the study was relatively small. Therefore, future studies assessing different muscle groups in a larger population with post-stroke spasticity, using multiple US scanners with standardized technique, is warranted.

8. CONCLUSION

This is the first study evaluating the effect of BoNT-A on muscle spasticity following stroke by mean of SWE and with the comparison of sEMG data.

We demonstrated a reduction of muscular stiffness and spasticity, all related to neural-mediated hypertonus decrease. In particular, we demonstrated that, in trained hands and with a positioning of the probe along the direction of muscular fibers, SWE is effective for the assessment of stiffness decrease after BoNT-A therapy.

Nevertheless, stretch reflex assessed by sEMG improves more than SWE-assessed muscular stiffness because this last technique also encompasses in its measurements the structural involutive changes of paretic muscles other than neural-mediated spasticity. At T0 in non-stretched conditions when electromyographic activity is reduced and, moreover at T1 when botulinum toxin treatment abolishes spasticity and spastic dystonia, SWE driven comparison between the spastic muscle and the contralateral unaffected homologous one may disclose the amount of stiffness due only to intrinsic muscular involutive remodelling.

Alongside sEMG, shear wave elastography could therefore constitute an added-value to clinicians who manage spasticity for the assessment of responses to treatments and monitoring therapeutic interventions.

List of Tables

List of Figures

spring-shaped gure shown in the left bottom of both the elastograms indicates that the pressure the operator performed with the transducer was appropriate to produce an adequate stress to get the elastogram.

Fig. 10. *Shear wave elastography*. The focused US beam pushed by the US probe generates shear waves into the target tissue (left); their velocities are detected by the same transducer and represented on the B-mode image (right) by a superimposed colour-coded map in which (in this case) the lower values are depicted in blue and the higher ones in red, giving a quantitative analysis of tissutal stiffness (higher speeds in stiffer tissues and viceversa).

Fig. 11. *SWE of rectus femoris muscle*. After the generation of the 'pushing' beam by the transducer, the values of the shear modulus in the targeted area are represented by mean of a colour-coded map set as represented by the coloured bar on the left of the screen. It is possible to get also a quantitative analysis of the investigated tissue by placing some ROIs (with modificable dimensions) over the map and get the corresponding value at the left bottom angle of the screen. Note that, on the right elastographic map, the stiffer areas in the centre of the map correspond to the central rectus femoris aponeurosis.

Fig. 12. *SWE assessment with transverse orientation of the probe*. Scheme illustrating SWE acquisition on short axis of muscular fibers: the transducer is placed on muscular belly performing consecutive transverse scans with the aim of assess the maximum amount of muscle (left); in each scan SW velocities are measured in the positioned ROI generating the relative color-coded elastogram superimposed to the B-mode image (right). A final mean value is then expressed.

Fig. 13. *SWE assessment with longitudinal orientation of the probe*. Scheme illustrating SWE acquisition on long axis of muscular fibers: the transducer is placed on muscular belly performing consecutive longitudinal scans with the aim of assess the maximum amount of muscle (left); in each scan SW velocities are measured in the positioned ROI generating the relative color-coded elastogram superimposed to the B-mode image (right). A final mean value is then expressed.

Fig. 14. *Modified Heckmatt scale*. Normal background echogenicity with clearly internal septa (I); increase in background echogenicity while intramuscular septa are still definable (II); 3. increase in background echogenicity and less definable septa (III); increase in background echogenicity without definable septa (IV).

Fig. 15. *sEMG results*. Chart illustrating the electromyographic activity (μV) measured in spastic muscles before (T0) and 4 weeks after (T1) botulinum toxin A injection at muscle relaxation (spastic dystonia) and during passive extension (spasticity).

Fig. 16. *MAS scores*. Chart illustrating the significant difference in MAS scores assessments of spastic muscles before (T0) and 4 weeks after (T1) botulinum toxin A injection.

Fig. 17. *SWE reduction between T0 and T1*. In the upper-right quadrant is illustrated an example of an elastogram (superimposed to the B-mode image) generated by a ROI placed in biceps brachii muscular belly along the direction of the fibers at T0; in the lower right image the same evaluation at T1 shows lower values (lower left corners of the images). Images on the upper- and lower-left quadrant are the correspective B-mode conventional US image automatically paired on the screen by the SEL software.

Fig. 18. *SWE difference between transverse and longitudinal assessments*. In the upper-right quadrant is illustrated an example of an elastogram (superimposed to the B-mode image) generated by a ROI placed in a non-paretic, non-stretched biceps brachii muscular belly across the direction of the fibers; in the lower right image the elastogram generated along the direction of muscular fibers of the same muscle shows higher values expressed both qualitatively with different-coloured map and quantitatively in m/s (lower left corners of the images). Images on the upper- and lower-left quadrant are the correspective B-mode conventional US image automatically paired on the screen by the SEL software (transverse US scan in the upper-left quadrant and longitudinal US scan in the lower-left quadrant).

Fig. 19. *Spastic muscles SWE speeds*. Chart illustrating SWE velocities assessed in paretic muscles at T0 and T1; significant difference ($p<0.05$) found in longitudinal assessments (group Bp and Dp).

Fig. 20. *Non-paretic muscles SWE speeds*. Chart illustrating SWE velocities assessed in non-paretic muscles at T0 and T1; only a slight significant difference (p:0.04) found in group B.

Fig. 21. *MHS grade II*. Conventional US appearance of biceps brachii and brachial muscles on non-paretic (NP) and paretic side (P) following stroke: on the left image normal US appearance of muscle with regular echogenicity of fibers and normal muscular fibers - intrasmuscular septa differentiation; the right image shows volume reduction of muscle and increase in background echogenicity with intramuscular septa more represented but still well definable.

Fig. 22. *MHS grade III*. Conventional US appearance of biceps brachii and brachial muscles on non-paretic (NP) and paretic side (P) following stroke, as assessed with longitudinal US scans: on the left image normal US appearance of muscle with regular echogenicity of fibers and normal muscular fibers - intrasmuscular septa differentiation; the right image shows volume reduction of muscle and significant increase in background echogenicity with intramuscular septa more represented and less definable.

Acknowledgements

I would like to express my deepest gratitude to Lucio Marinelli MD, PhD, for his tutoring and to Prof. Luca Maria Sconfienza MD, PhD, for his continuous teaching and support.

Special thanks go to Laura Privitera MD, Riccardo Pedrini MD and William Campanella MD, for their contribution to patients recruitment.

Notes

Chapter I - II widely refer to 'Silvestri E, Muda A, Orlandi D. 2015. Ultrasound Anatomy of Lower Limb Muscles. Springer International Publishing' & to 'Silvestri E, Martino F, Puntillo F. 2018. Ultrasound-Guided Peripheral Nerve Blocks. Springer International Publishing AG.

Chapter III widely refers to Trompetto C et al. Pathophysiology of spasticity: implications for neurorehabilitation. Biomed Res Int. 2014:354906.

BIBLIOGRAPHY

Altahhan KN, Wang Y, Sobh N, Insana MF. Indentation measurements to validate dynamic elasticity imaging methods. Ultrason Imaging. 2016;38 (5), 332–345.

Bamber J, Cosgrove D, Dietrich CF, Fromageau J, Bojunga J, Calliada F, et al. EFSUMB guidelines and recommendations on the clinical use of ultrasound elastography. Part 1: basic principles and technology. Ultraschall in der Medizin. 2013;34, 169–184.

Barr RG, Ferraioli G, Palmeri ML, Goodman ZD, Garcia-Tsao G, Rubin J, et al. Elastography Assessment of Liver Fibrosis: Society of Radiologists in Ultrasound Consensus Conference Statement. Radiology 2015;276 (3), 845–861.

Bercoff J, Tanter M, Fink M. Supersonic shear imaging: a new technique for soft tissue elasticity mapping. IEEE transactions on ultrasonics, ferroelectrics, and frequency control. 2004; 51 (4), 396–409.

Bohannon RW, Smith MB. Interrater reliability of a modified Ashworth scale of muscle spasticity. Phys. Ther. 1987; 67 (2), 206–207.

Brandenburg JE, Eby SF, Song P, Zhao H, Brault JS, Chen S, An K-N. Ultrasound elastography: the new frontier in direct measurement of muscle stiffness. Arch. Phys. Med. Rehabil. 2014;95 (11), 2207–2219.

Brin M, Childers M, Esquenazi A. Dosing, administration, and a treatment algorithm for use of botulinum toxin A for adult-inset-spasticity. Muscle Nerve 1997;6:S208–S220.

Burke, B., Wissel, J., Donnan, G.A. Pathophysiology of spasticity in stroke. Neurology. 2013;80 (Suppl. 2), S20–S26

Chen J, O'Dell M, He W, Du LJ, Li PC, Gao J. Ultrasound shear wave elastography in the assessment of passive biceps brachii muscle stiffness: Influence of sex and elbow position. Clin. Imaging. 2017;45, 26–29.

Creze M, Nordez A, Soubeyrand M, Rocher L, Maître X, Bellin M-F. Shear wave sonoelastography of skeletal muscle: basic principles, biomechanical concepts, clinical applications, and future perspectives. Skeletal Radiol. 2018; 47, 457–471.

Dorado Cortez C, Hermitte L, Ramain A, Mesmann C, Lefort T, Pialat JB. Ultrasound shear wave velocity in skeletal muscle: a reproducibility study. Diagn Interv Imaging. 2016;97(1):71–9.

Dubois G, Kheireddine W, Vergari C, Bonneau D, Thoreux P, Rouch P, et al. Reliable protocol for shear wave elastography of lower limb muscles at rest and during passive stretching. Ultrasound Med Biol. 2015;41(9):2284–91.

Eby S, Zhao H, Song P, Vareberg BJ, Kinnick R, Greenleaf JF, An K-N, Chen S, Brown AW. Quantitative Evaluation of Passive Muscle Stiffness in Chronic Stroke. Am. J. Phys. Med. Rehab. 2016;95, 899–910.

Eby SF, Song P, Chen S, Chen Q, Greenleaf JF, An KN. Validation of shear wave elastography in skeletal muscle. J Biomech. 2013;46(14):2381–7.

Eby S, Zhao H, Song P, Vareberg BJ, Kinnick RR, Greenleaf JF, An K-N, Brown AW, Chen S. Quantifying spasticity in individual muscles using shear wave elastography. Radiol. Case Rep. 2017;12, 348–352.

Faist M, Berger W, Dietz V. Changes in mechanical muscle fibre properties may contribute to spastic muscle hypertonia. Ann Rehabil Med Phys 1999;42:493–496.

Feigin VL, Norrving B, Mensah GA. 2017. Global burden of stroke. Circ. Res. 120 (3), 439–448.

Francisco GE, McGuire JR. Poststroke spasiticity management. Stroke. 2012;43, 3132–3136.

Gao J, Chen J, O'Dell M, Li PC, He W, Du LJ, Rubin JM, Weitzel W, Min R. Ultrasound strain imaging to assess the biceps brachii muscle in chronic poststroke spasticity. J Ultrasound Med 2018a;37:8.

Gao J, He W, Du L-J, Chen J, Park D, Wells M, Fowlkes B, O'Dell M. Quantitative ultrasound imaging to assess the biceps brachii muscle in chronic post- stroke spasticity: Preliminary observation. Ultrasound Med. Biol. 2018;44 (9), 1931–1940.

Gao J, Rubin JM, Chen J, O'Dell M. Ultrasound elastography to assess botulinum toxin A treatment for post-stroke spasticity: A feasibility study. Ultrasound Med. Biol. 2019(0), 1–9.

Gennisson JL, Deffieux T, Mace E, Montaldo G, Fink M, Tanter M. Viscoelastic and anisotropic mechanical properties of in vivo muscle tissue assessed by supersonic shear imaging. Ultrasound Med. Biol. 2010;36 (5), 789–801.

Ghai A, Garg N, Hooda S, Gupta T. Spasticity - Pathogenesis, prevention and treatment strategies. Saudi J. Anaesth. 2013;7(4), 453–460.

Gracies J-M. "Pathophysiology of spastic paresis. I: paresis and soft tissue changes," *Muscle and Nerve*, vol. 31, no. 5, pp. 535–551, 2005.

Hermens HJ. European recommendations for surface ElectroMyoGraphy: results of the SENIAM project. In: Roessingh Research and Development BV, editor. Enschede: Roessingh Research and Development; 1999 (SENIAM).

Hoyt K, Kneezel T, Castaneda B, Parker KJ. Quantitative sonoelastography for the in vivo assessment of skeletal muscle viscoelasticity. Phys Med Biol. 2008;53(15):4063–80.

Hug F, Tucker K, Gennisson JL, Tanter M, Nordez A. Elastography for muscle biomechanics: toward the estimation of individual muscle force. Exerc Sport Sci Rev. 2015;43(3):125–33.

Jakubowski KL, Terman A, Santana RVC, Lee SSM. Passive material properties of stroke-impaired plantarflexor and dorsiflexor muscles. Clin. Biomech. 2017; 49, 48–55.

Kesikburun S, Yaşar E, Adıgüzel E, Güzelküçük Ü, Alaca R, Tan A.K. Assessment of Spasticity With Sonoelastography Following Stroke: A Feasibility Study. 2015; PM &R. 7 (12), 1254–1260.

Klauser AS, Miyamoto H, Bellmann-Weiler R, Feuchtner GM, Wick MC, Jaschke WR. Sonoelastography: musculoskeletal applications. Radiology. 2014;272(3):622-33.

Kuo CL, Hu GC. Post-Stroke Spasticity: A Review of Epidemiology, Pathophysiology, and Treatments. Int. J. Gerontol. 2018;12 (4), 280–284.

Lance JW. 1980. Symposium. In: Young, R.R., Koella, W.P. (Eds.), Spasticity: Disordered Motor Control. eds Feldman R. G. Year Book Medical Pubs, Chicago, pp. 485–495.

Le Sant G, Nordez A, Hug F, Andrade R, Lecharte T, McNair P, Gross R. Effect of stroke injury on the shear modulus of the lower leg muscle during passive dorsiflexion. J. appl. Physiol. 2018;126 (1), 11–22.

Lee SSM, Spear S, Rymer WZ. Quantifying changes in material properties of stroke-impaired muscle. Clin. Biomech. 2015;30, 269–275.

Lee SSM, Jakubowski KL, Spear SC, Rymer WZ. Muscle material properties in passive and active stroke-impaired muscle. J. Biomech. 2019;83, 194–204.

Lerner RM, Huang SR, Parker KJ. “Sonoelasticity” images derived from ultrasound signals in mechanically vibrated tissues. Ultrasound Med. Biol. 1990;16 (3), 231–239.

Liber RL, Steinman S, Barash IA, Chambers H. Structural and functional changes in spastic skeletal muscle. Muscle Nerve. 2004;29, 267–615.

Li S, Francisco GE. New insights into pathophysiology of post-stroke spasticity. Front Hum Neurosci 2015;9:192.

Marinelli L, Currà A, Trompetto C, Capello E, Serrati C, Fattapposta F, et al. Spasticity and spastic dystonia: the two faces of velocity-dependent hypertonia. J Electromyogr Kinesiol. 2017 Dec;37:84-89.

Marinelli L, Trompetto C, Mori L, Vigo G, Traverso E, Colombano F, Abbruzzese G. Manual linear movements to assess spasticity in a clinical setting. PLoS One. 2013;8(1):e53627.

Mathevon L, Michel F, Aubry S, Testa R, Lapole T, Arnaudeau LF, Fernandez B, Parrate B, Calmels P. Two-dimensional and shear wave elastography ultrasound: A reliable method to analyse spastic muscles? Muscle Nerve. 57, 2018. 222–228.

Meriam, JL, Kraige LG. 2012a (A). Engineering mechanics. Volume 1. Statics 7th (seventh) Edition. New York: Wiley.

Meriam JL, Kraige LG. 2012b (B). Engineering mechanics. Volume 2. Dynamics 7th (seventh) Edition. New York: Wiley.

Miyamoto N, Hirata K, Kanehisa H, Yoshitake Y. Validity of measurement of shear modulus by ultrasound shear wave elastography in human pennate muscle. PLoSOne. 2015;10(4): e0124311.

Nightingale, K.Acoustic Radiation Force Impulse (ARFI) Imaging: a Review. Curr Med Imaging Rev. 2011;7(4), 328–339.

Ophir, J., Cespedes, I., Ponnekanti, H., Yazdi, Y., Li, X. Elastography: a quantitative method for imaging the elasticity of biological tissues. Ultrason Imaging. 1991;13 (2), 111–134.

Pandyan, A.D., Gregoric, M., Barnes, M.P., Wood, D., van Wijck, F., Burridge, J., Hermens, H., Johnson, G.R. Spasticity: Clinical perceptions, neurological realities and meaningful measurement. Disability and Rehabilitation. 2005;27, 2–6.

Pandyan AD, Price CI, Barnes MP, Johnson GR. A biomechanical investigation into the validity of the Modified Ashworth Scale as a measure of elbow spasticity. Clin Rehabil 2003;17: 290–293.

Phan A, Lee J, Gao J. Ultrasound shear wave elastography in assessment of skeletal muscle stiffness in senior volunteers. Clin Imaging. 2019 Nov - Dec;58:22-26.

Pillen S. Skeletal muscle ultrasound. Eur. J. Transl. Myol. 2010;1 (4), 145–155.

Rasool G, Wang AB, Rymer WZ, Lee SSM. Shear Waves Reveal Viscoelastic Changes in Skeletal Muscles After Hemispheric Stroke. IEEE Trans. Neural Syst. Rehabilitation Eng. 2018; 26 (10), 2006–2014.

Šarabon N, Kozinc Ž, Podrekar N. Using shear-wave elastography in skeletal muscle: a repeatability and reproducibility study on biceps femoris muscle. PLoS One. 2019 Aug 30;14(8):e0222008.

Sheean G. " The pathophysiology of spasticity," European Journal of Neurology, vol. 9, supplement 1, pp. 3–61, 2002.

Shiina, T., Nightingale, K.R., Palmeri, M.L., Hall, T.J., Bamber, J.C., Barr, R.G., et al. WFUMB guidelines and recommendations for clinical use of ultrasound elastography: Part 1: basic principles and terminology. Ultrasound in medicine & biology. 2015;41, 1126–1147.

Shin HJ, Kim MJ, Kim HY, Roh YH, Lee M-J. Comparison of shear wave velocities on ultrasound elastography between different machines, transducers, and acquisition depths: a phantom study. Eur. Radiol. 2016;26, 3361–3367.

Sigrist RMS, Liau J, Kaffas AE, Chammas MC, Willmann JK. Ultrasound Elastography: Review of Techniques and Clinical Applications. Theranostics. 2017;7 (5), 1303–1329.

Silvestri E, Muda A, Orlandi D. 2015. Ultrasound Anatomy of Lower Limb Muscles. Springer International Publishing.

Silvestri E, Martino F, Puntillo F. 2018. Ultrasound-Guided Peripheral Nerve Blocks. Springer International Publishing AG.

Sions JM, Tyrell CM, Knarr BA, Jancosko A, Binder-Macleod SA. Age- and stroke-related skeletal muscle changes: A review for the geriatric clinician. J. Geriatr. Phys. Ther. 2012;35(3),155–161.

Sommerfeld DK, Eek EU, Svensson AK, Holmqvist LW, von Arbin MH. Spasticity after stroke: Its occurrence and association with motor impairments and activity limitations. Stroke. 2004;35, 134–139.

Tang A, Cloutier G, Szeverenyi NM, Sirlin CB. Ultrasound Elastography and MR Elastography for Assessing Liver Fibrosis: Part 2, Diagnostic Performance, Confounders, and Future Directions. Am. J. Roentgenol. 2015;205(1),33–40.

Thilmann AF, Fellows SJ, Garms E. The mechanism of spastic muscle hypertonus: variation in reflex gain over the time course of spasticity. Brain 1991;114:233–244.

Trompetto C, Currà A, Puce L, Mori L, Serrati C, Fattapposta F, Abbruzzese G, Marinelli L. Spastic dystonia in stroke subjects: prevalence and features of the neglected phenomenon of the upper motor neuron syndrome. Clin Neurophysiol. 2019 Apr;130(4):521-527.

Trompetto C, Marinelli L, Mori L, Pelosin E, Currà A, Molfetta L, Abbruzzese G. Pathophysiology of spasticity: implications for neurorehabilitation. Biomed Res Int. 2014;2014:354906.

Trompetto C, Marinelli L, Puce L, Mori L, Serrati C, Fattapposta F, Currà A. "Spastic dystonia" or "Inability to voluntary silence EMG activity"? Time for clarifying the nomenclature. Clin Neurophysiol. 2019 Jun;130(6):1076-1077.

Vill K, Schessl J, Teusch V, Schroeder S, Blaschek A, Schoser B, Müller-Felber W. Muscle ultrasound in classic infantile and adult Pompe disease: a useful screening tool in adults but not in infants. Neuromuscul Disord. 2015 Feb;25(2):120-6.

Yaşar E, Adigüzel E, Kesikburun S, Yenihayat I, Yilmaz B, Alaca R, Tan AK. Assessment of forearm muscle spasticity with sonoelastography in patients with stroke. Br J Radiol. 2016;89(1068):20160603.

Wu CH, Ho YC, Hsiao MY, Chen WS, Wang TG. Evaluation of post-stroke muscle stiffness using shear wave ultrasound elastography. Ultrasound Med. Biol. 2017;43(6),1105–1111.